2017

The Effects of Linoleic Acid on Rubidium Uptake by Sodium Potassium Pumps in Rat Myocardial Cells

Mohammed Ahmed Gaafarelkhalifa
Minnesota State University, Mankato

The Effects of Linoleic Acid on Rubidium Uptake by Sodium Potassium Pumps in Rat Myocardial Cells

By

Mohammed A. Gaafarelkhalifa

Mentored by

Dr. Michael Bentley

A Thesis Submitted in Partial Fulfillment of the Requirements for the Degree of Master of Science in Biology

Minnesota State University, Mankato

Mankato, Minnesota

November 9th, 2017

November 7th, 2017

The Effects of Linoleic Acid on Rubidium Uptake by Sodium Potassium Pumps in Rat Myocardial Cells

Mohammed Gaafarelkhalifa

This thesis has been examined and approved by the following members of the student's committee.

_____
Dr. Michael Bentley
Advisor

_____
Dr. Penny Knoblich
Committee Member

_____
Dr. David Sharlin
Committee Member

Abstract

The Effects of Linoleic Acid on Rubidium Uptake by Sodium Potassium Pumps in Rat Myocardial Cells

Name: Mohammed Gaafarelkhalifa

Degree: Master of Biology

Institution: Minnesota State University, Mankato

Date of Submission: November 9th, 2017

Congestive Heart failure is amongst the leading causes of death in the United States. It is treated through a variety of different therapeutic targets including the inhibition of sodium potassium pumps. Drugs currently used in this pathway of treatment such as Digitalis have adverse toxic effects. This study examines the inhibitory effects of linoleic acid (L.A) on sodium potassium pumps in isolated rat cardiomyocytes using the incorporation of rubidium detected by SEM/EDS technology as the index for sodium-potassium pump activity. Isolated heart cells were incubated in the following treatments: Rb-Krebs buffer without treatment (negative control), Ouabain+ Rb-Krebs buffer (positive control), 10^{-3} M L.A+ Rb-Krebs buffer, and 10^{-6} M L.A+ Rb-Krebs buffer. The results established Rb-Krebs as the negative control with a mean of 1.279 +/- 0.075 for Rb % average of 10 replicates with 10 cells analyzed in each replicate. Ouabain + Rb-Krebs was established as the positive control for inhibition of rubidium uptake with a mean value of 0.701 +/- 0.073. It was found that the 10^{-6} M, and not 10^{-3} M, concentration of linoleic acid exhibited inhibitory effects of rubidium uptake with a mean value of 0.805 +/- 0.121 and 0.903 +/- 0.095, respectively.

Acknowledgements

I am pleased, honored, and forever-thankful to have had Dr. Michael Bentley as my thesis advisor, and I am sincerely grateful for all of his mentoring, support and teachings throughout my research experience in his lab. I would like to also genuinely thank my committee members Dr. David Sharlin for teaching me “How to research” and providing me with endless support and extremely valuable techniques, and Dr. Penny Knoblich for teaching me all that I know about cardiovascular physiology and for generously providing me with laboratory equipment throughout my research. Lastly, I would like to thank the Department of Biological Sciences for granting me this wonderful opportunity, and for providing me with financial and facility support and resources.

Table of Contents

Introduction

The sodium potassium ATPase, also known as the sodium potassium pump, is a cellular membrane protein located in all animal cells (2). Its main function is to transport potassium ions into the cell and to transport sodium ions out against their respective concentration gradients. This action serves the cell directly in several ways such as maintenance of cell volume, allowing the cells to create a cellular membrane resting potential, and serving as a transducer for cellular signals (2). Indirectly, functions of the sodium potassium pump include interactions which couple its activity with specialized cellular processes. One such interaction couples the pump's activity with the sodium-calcium exchange (NCX) channel (2). Calcium ions are necessary for cardiomyocytes (heart muscle cells) to generate heart muscle contractions (10).

Inhibition of sodium potassium pump activity has been a treatment route for congestive heart failure (CHF) (10). This inhibition requires specific molecules such as glycosides (23), for example digoxins and Ouabain, which have been used as prescription medicine and home remedies, respectively, to treat heart failure and other heart problems for over 200 years (10). The therapeutic dose range for digoxins, pharmaceutically recognized as digitalis, is narrow, falling between 0.8 -1.8 ng/ml of blood (19). CHF patients under digoxin treatment face issues of drug toxicity. Moreover, digoxins may exhibit drug-to-drug interactions with drugs that relieve symptoms and complications of CHF (8). Such drugs include diuretics used to relieve fluid retention and may exacerbate digoxin toxicity. Symptoms of digoxin toxicity include gastrointestinal complications, arrhythmias, and breathing difficulty amongst many other severe symptoms (23).

Linoleic acid is a naturally occurring fatty acid derived from several plants including *Nigella sativa*. *Nigella sativa* has been a staple of traditional medicine for centuries (1). Often ingested orally, the seeds of *Nigella sativa* are used to alleviate a

variety of different aliments including respiratory infections and hypertension (1). Early studies suggest that linoleic acid inhibits sodium potassium pumps (12, 25). Toxicologically, linoleic acid appears to be safe for human consumption, and is included in a variety of dietary supplements (27). It exhibits no apparent toxic effects in doses as high as 3.2 grams of linoleic acid per kilogram of body mass. However, it is important to note that linoleic acid has a variety of chemically produced isomers and metabolic derivatives, some of which have toxic effects (27). The most biologically-active linoleic acid isomers, cis-9,trans-11 and trans-10,cis-12 isomers, are considered safer for human consumption (30) and are used in this study.

The hypothesis of this thesis is that linoleic acid decreases sodium potassium pump activity. The pump activity was determined by cardiomyocyte rubidium weight percentages. Rubidium is a congener for potassium and is actively transported into heart muscle cells by sodium potassium ATPase (18, 21). Furthermore, cardiomyocyte rubidium weight percent may be measured by Scanning Electron Microscopy (SEM) and Energy Dispersive Spectroscopy (EDS) (4, 18, 21).

There were four main experimental objectives in this thesis. First, isolation of viable adult rat cardiomyocytes by the digestive enzyme collagenase was optimized through preliminary trials. Second, cardiomyocyte rubidium weight percent over time was determined by using Scanning Electron Microscopy (SEM) and Energy Dispersive Spectroscopy (EDS). Third, inhibitory effect of Ouabain on rubidium uptake was determined by a decrease in cardiomyocyte rubidium weight percentages through SEM and EDS analysis. Finally, the effect of linoleic acid on cardiomyocyte rubidium weight percent was determined.

Literature Review

Congestive Heart Failure

Congestive heart failure, CHF, is a cardiovascular condition where the heart ventricles are not able to adequately pump blood due to cardiac tissue damage, restrictions in coronary flow, or any conditions resulting in the mechanical dysfunction of the cardiac pump (26). Heart failure could occur during both of the major stages of the cardiac cycle, cardiac systole and cardiac diastole (26). Failure during cardiac systole causes insufficient contraction resulting in decreased ejection fraction, or the fraction of stroke volume divided by end diastolic volume (26). Diastolic heart failure, on the other hand, is the inability of the ventricle to relax or dilate sufficiently to accommodate for proper cardiac filling resulting in a decreased end diastolic volume (EDV), which in turn decreases the overall cardiac output (26).

Heart failure often occurs in one side of the heart so that the failed side increases the workload and demands of the still healthy side, which eventually leads to its failure (26). Right-sided heart failure results in the right ventricle being unable to generate forceful enough contractions to pump the blood it receives from the systemic (body) circulation via the right atrium (26). As a result, there is a backup of fluids and elevated venous pressure, causing fluid retention in organs, bodily fatigue and edema (26). Left-sided heart failure results in the left ventricle being unable to pump the blood it receives from the pulmonary circulation via the left atrium (26). As a result, hydrostatic pressure in pulmonary capillary beds is elevated, causing vascular fluid leakage into pulmonary tissues (26). In either-sided heart failure, the progression of the disease is difficult for the patients as they struggle to perform basic functions and movements. The heart is unable to keep up with the increasing demand, and depending on the overall level of fitness and

health of the patient, intrinsic and extrinsic factors may further compound the severity of congestive heart failure symptoms (26).

Today, and with the increase in age span and the emergence of age related diseases, heart disease is at the top of the charts as the number one leading cause of death in the United States (11). In 2010, the American Heart Association reported that 5.1 million individuals were diagnosed as CHF patients in the United States (11). Half of CHF patients die within five years of diagnosis (11). In 2009, Centers for Disease Control (CDC) reported that one out of every nine deaths had CHF as the main or contributing cause of death (11). Treatment of CHF in the United States costs an approximate $32 billion each year (19).

There are two main treatment avenues for patients with CHF: 1) life style changes, and 2) pharmaceuticals. Physicians often promote life style changes as the main mode of treatment and first line of defense against CHF. Those lifestyle changes include cessation of smoking, drug use, and ethanol consumption (34). Individuals are also put on a carful diet and an exercise regimen to rehabilitate their cardiovascular system. Studies have shown that these changes lead to gradual but significant improvement in cardiac function (34). The success of such program depends on the extent and stage of the heart failure, but also it depends and the compliance and willingness of the patients to conform to the program. Unfortunately, patients often revert to their old lifestyles after a brief period of change (34). That complicates their recovery process and renders the heart failing once again. Medical doctors then introduce the more aggressive form of treatment, pharmaceuticals.

There are three main classes of pharmaceuticals used for treating CHF: vasodilators, diuretics, and sodium potassium pump inhibitors (29). Vasodilators are compounds that widen blood vessels throughout the body (26). They relieve CHF by

widening coronary arteries to enhance cardiac function by distributing oxygen rich blood to heart tissue, and by widening systemic and pulmonary arteries and reducing the workload on heart muscle (26). A second class of pharmaceuticals used to treat CHF is diuretics. This class of pharmaceuticals increases the excretion rate of bodily fluids through urine, relieving patients of edema and retained fluids in organs, including the congestion of lungs (29). A third class of pharmaceuticals is sodium potassium pump inhibitors. This thesis will focus on the inhibition of the sodium-potassium pump and will provide the rationale for proposing linoleic acid as an inhibitor of the pump.

Sodium Potassium Pump

The sodium potassium adenosine triphosphatase, commonly referred to as the sodium potassium pump, is a transmembrane protein with one end of the protein exposed to the extracellular side and the other end is projected into the cell interior (2). The composition of the pump varies among specialized cells and among species. The most conserved components or protein domains are the α-subunit and β-subunit, but there are several isoforms of these subunits (10). The α-subunit serves as the binding site for the various molecules interacting with the pump including ATP, and it carries catalytic functions. The β-subunit spans across the membrane and it contains amino acid residues providing stability to the channel within the hydrophobic inners of the lipid bilayer (10).

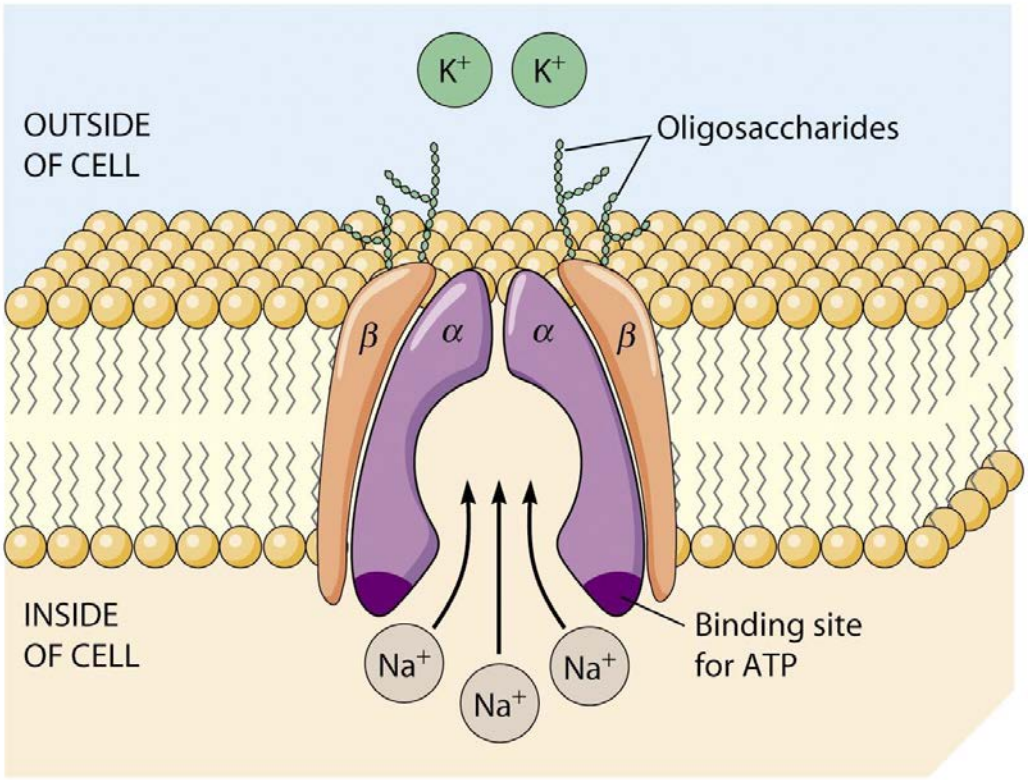

Figure 1: A diagram showing the structure of sodium potassium ATPase. Obtained from (http://www.mun.ca/biology/desmid/brian/BIOL2060/BIOL2060-07-08/08_11.jpg)

The sodium potassium pump (Figure 1) works in cycles including conformational changes of the pump, binding and release of phosphate groups, sodium, and potassium ions. In its original conformation, the pump has a sodium-binding site exposed intracellularly (2). Once three sodium ions bind, an adenosine triphosphate (ATP) is recruited at the α-subunit's catalytic site where the energetic phosphate group is cleaved off and linked to the pump (2). The remaining adenosine diphosphate (ADP) is released. The energy harnessed from the energetic phosphate linkage drives a conformational change of the pump where the sodium-binding site is now exposed to the extracellular matrix, and the sodium ions are ejected out of the cell (2). At this conformation, the potassium binding site is exposed extracellularly. This conformation is also known as the E2P conformation of sodium potassium pumps. At this stage of the cycle, two potassium ions bind, which causes the release of the linked phosphate group (2). The release of the

phosphate group allows the pump to return to its original conformation, and thus exposing the potassium-binding site intracellularly (2). Potassium ions are released, and sodium ions are recruited to restart the cycle once again. The entirety of the cycle occurs in 10 milliseconds of time (2). The activity of sodium potassium pumps allows the cell to maintain a gradient of Na^+ and K^+ ions in both the extracellular and intracellular vicinity of a cellular membrane. This gradient of ions serves many functions including regulating osmotic pressure (or pressure created by water molecules) inside the cell, and by influencing the activity of other membrane channels or pumps (2). For example, extracellular Na^+ ions drive the removal of excess intracellular calcium ions through the sodium calcium exchange (NCX) channel (28).

Calcium and Muscle Cell Contraction

Calcium ions bind to many cellular proteins and affect their shape and functions, and therefore, intracellular calcium levels are highly regulated. For example, calcium is a major component in the excitation-contraction coupling pathway, as seen in cardiomyocytes (26). This pathway describes the movement of an action potential between neighboring cardiomyocytes, and the release of calcium from the sarcoplasmic reticulum of an excited cell into its intracellular space to develop a contraction (26). As part of this pathway, a relatively small amount of Ca^{2+} ions rush into a cardiomyocyte through T tubules in the cellular membrane. Once inside a cardiomyocyte, the calcium ions trigger the release of a much larger concentration of calcium ions from the sarcoplasmic reticulum (SR) (26). Calcium is actively pumped into the SR during refractory periods, periods in which the cardiac muscle is non-responsive to electrical stimuli and is not contracting (10). Once released from the SR onto the cytoplasm, calcium binds and activates proteins responsible for contracting a cell (26). Increases in

the number of calcium ions binding proteins responsible for contracting a cell leads to the development of more forceful cardiac contractions. Since the process of heart contraction is highly sensitive and rhythmic, cardiac cells naturally work to maintain lower concentration of free cytoplasmic calcium. Notably, the sodium-potassium pump couples its activity with NCX is a key regulatory measure for the removal of free cytoplasmic calcium (28).

Glycosides and Enzymatic Inhibition

Enzyme inhibition is the process where a molecule, not the usual substrate, binds the enzyme in a manner that renders the enzyme unable to carry out its enzymatic function. In the case of sodium potassium pumps, inhibition stops the pump from moving potassium into the cell and sodium out of it (2). In myocardial sodium potassium pumps, such inhibition leads to a decreased concentration gradient for sodium to move into the cell (Figure 2). This inhibition also decreases NCX activity, and decreases removal rate of cytoplasmic calcium to the extracellular matrix (10). Therefore, when the sodium potassium pump is inhibited and intracellular calcium levels rise, more forceful cardiac contractions are generated (10). This coupled inhibition and increased number of calcium ions provides the basis for treatment of CHF by inducing more forceful heart contractions and increase overall cardiac output.

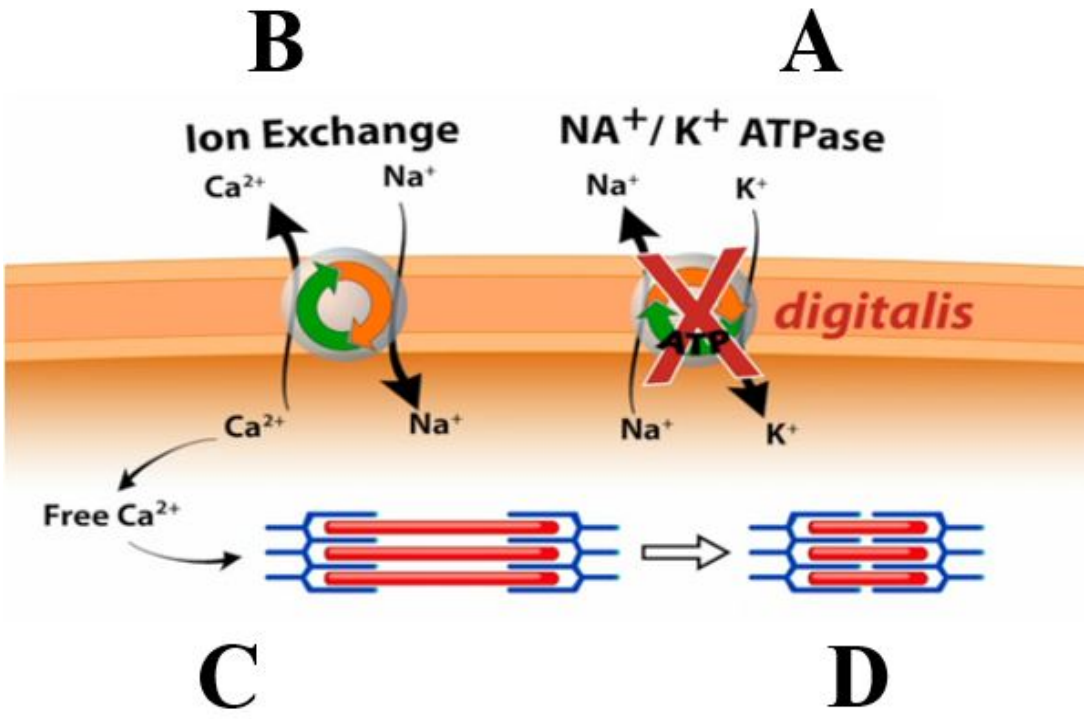

Figure 2: Digitalis mechanism of action where **A)** digitalis binds sodium-potassium pump, **B)** sodium-calcium exchange channel utilizes extracellular sodium pumped by sodium-potassium pumps to drive calcium out of the cell, **C)** decreased extracellular sodium due to inhibition of sodium-potassium pump by digitalis causes increase in free calcium that binds relaxed sarcomere, and **D)** calcium binding of sarcomere causes contraction. Obtained from (https://quizlet.com/24869073/dit-cardiovascular-1-11-flash-cards/).

Glycosides, such as Ouabain and digoxins, are one class of sodium potassium pump inhibitors. They are aromatic chains of molecules containing a carboxyl terminal end (Figure 3) (22). Digoxin as a compound has a molecular mass of 780.9, and Ouabain has a molecular mass of 728.77 (22). These two inhibitor molecules have many similarities both in their chemical and physical make-up. They both inhibit the binding of potassium and lock the sodium potassium pump at the E2P conformation (2).

Linoleic Acid as an Inhibitor

Nigella sativa, also known as “the black seed” (Figure 4), has been widely and historically used as a remedy for a variety of ailments ranging from respiratory infections

to cardiovascular conditions such as hypertension and what is now diagnosed as CHF (1, 27). One active constituent of the seed appears to be linoleic acid (25). Loregeril et. al showed a significant decrease in the reoccurrence of myocardial infarction (MI) in survivors undergoing a Mediterranean diet rich in linoleic acid compared to survivors not on the diet (24). Linoleic acid is an 18 carbon conjugated fatty acid chain, meaning it has a stretch of alternating single and double bonds (Figure 3) (22). This conjugation allows the formation of isomers of the compound associated with the double bonds. Linoleic acid is an essential fatty acid that is metabolized into many biologically-active isomers involved in diverse range of physiological and pathological pathways (24). Linoleic acid metabolites are chemical derivatives containing one or multiple chemical groups added to the hydrocarbon chain or directly interacting with the carboxylic acid group (22). These derivatives exhibit varying conformational shapes, reactivity, and interactions with other molecules. For example, linoleic acid is a precursor in the formation of prostaglandins, and leukotrienes. Two of the most biologically-active linoleic isomers are the cis-9,trans-11 and trans-10,cis-12 (30). The linoleic acid used in this thesis was a mixture of these isomers.

Dietary levels of linoleic acid isomers are around 15-174 mg daily, primarily from meats and oils (24). Pharmacological studies have shown that dietary supplements of linoleic acid at doses between 1.8 g – 7 g is safe for human consumption and may help in fat loss and in reduction of blood pressure. However, additional benefits were not observed in doses above 3.4 (24).

Linoleic acid appears to interact with sodium potassium pumps. Mixtures of compounds extracted from Nigella sativa were used to determine their effect on sodium potassium pumps in pig kidney cells. The results indicated that there were two primary active constituents isolated from Nigella sativa that had inhibitory effects on sodium

pumps. Those two active constituents were oleic acid and linoleic acid (25). Ha et al. found that linoleic acid metabolites incorporated into the lipid bilayer and disrupted membrane fluidity (12). Their study found that the metabolites inhibited the sodium potassium pump. However, it was unclear whether the disruption of membrane fluidity was the single cause of the sodium potassium pump inhibition (12).

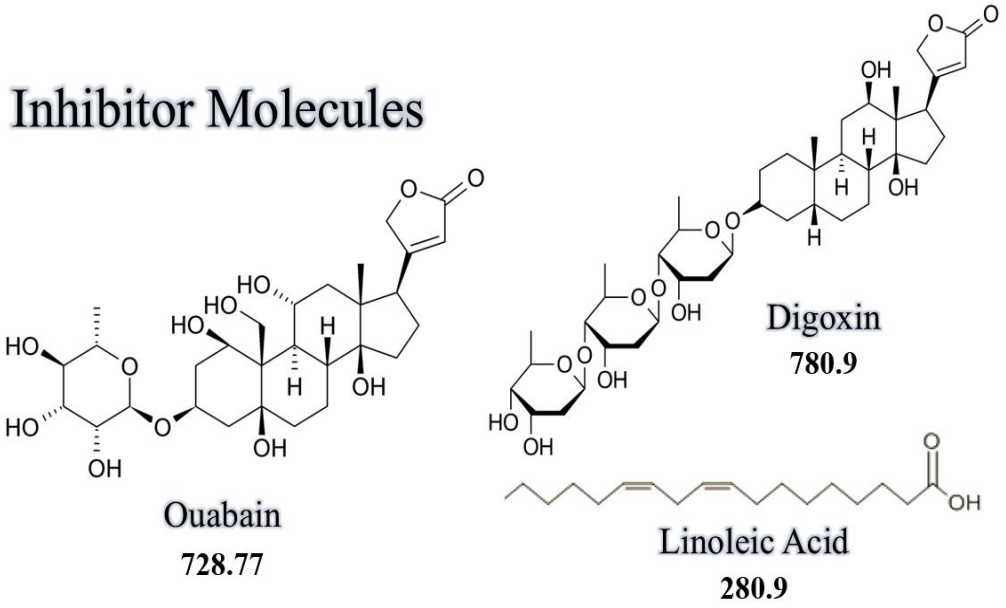

Figure 3: Chemical structures and molecular weight for Ouabain, Digoxin, and Linoleic Acid. Information in this figure is obtained from *PubChem.*

Figure 4: *Nigella sativa* plant (left panel), and the black seeds from the plant (right panel). Obtained from (https://www.gardenershq.com/flowerimage/Nigella-Sativa.jpg) and (http://changmoh.com/wp-content/uploads/2013/05/black_seed_healing-1.jpg)

Rubidium as a Potassium Congener

The element rubidium is an alkali metal of the first group within the periodic table (33). It lies a single period beneath potassium, and exhibits similar chemical properties and interactions. Potassium has an atomic mass of 39.09, an atomic radius of 235 picometer (pm), and atomic volume of 45.3 cubic centimeter per mole (cc/mol). Rubidium has an atomic mass of 85.46, an atomic radius of 248 pm, and an atomic volume of 55.9 cc/mol (33). Because rubidium is similar to potassium, is not normally found in the cell, and does not appear to have a harmful effect, it has been used as a tracer for potassium uptake into tissue via sodium potassium pump activity (4, 18, 21). Kupriyanov et al. used magnetic resonance imaging to determine the uptake of ^{87}Rb by pig hearts (21). Beck et al. infused rubidium chloride into kidney tissue and then used energy dispersive x-ray spectroscopy (EDS) to measure the incorporation of rubidium into kidney cells (4). Kalinowski infused rubidium *in vivo* into rats and subsequently used EDS to determine rubidium uptake in freeze dried rat muscles, hearts, and kidneys (18).

Langendorff Apparatus

The Langendorff apparatus provides a means to maintain viability of an excised heart (5). The basic Langendorff apparatus provides a means to infuse an oxygenated physiological solution into the coronary vasculature of the heart while maintaining temperature, and pressure. Solutions infused into the isolated heart are delivered through an aortic cannula inserted retrograde so that its tip is situated at the ostia of the coronary arteries (5). The retrograde infusion closes the aortic semilunar valve so that the perfusate flows into the coronary arteries (5).

Principles of Scanning Electron Microscopy

The scanning electron microscope is used to obtain surface views of cells and tissues utilizing electrons to create an image (15). This technology is based on the principle that a high energy, focused electron beam interacts with the object to cause a variety of emissions as illustrated in *Figure 5* (15). The scanning electron microscope (SEM) includes an electron gun, which is directed towards the sample. The electron beam, generated from the electron gun is focused on the sample by magnetic lenses as illustrated in *Figure 6*. As the electron beam excites the sample, secondary electrons are emitted from the surface of the sample. A detector gathers secondary electrons emitted by the excited sample (15). The signal from the detector is amplified and is converted into gray-scale values and displayed as an image on a monitor in synchrony with the scanning electron beam (15). In addition to electron emission, x-rays are also emitted from the sample and can be detected by energy dispersive spectroscopy (EDS) (15, 17).

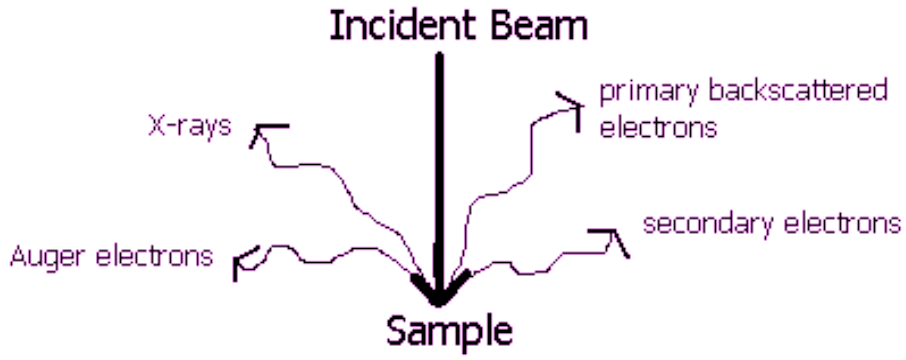

Figure 5: Types of emissions from a specimen excited by incident electron beam. Obtained from (http://ehs.virginia.edu/ehs/ehs.rs/rs.images/sem.incident.beam.coutesy.iowa.state.jpg).

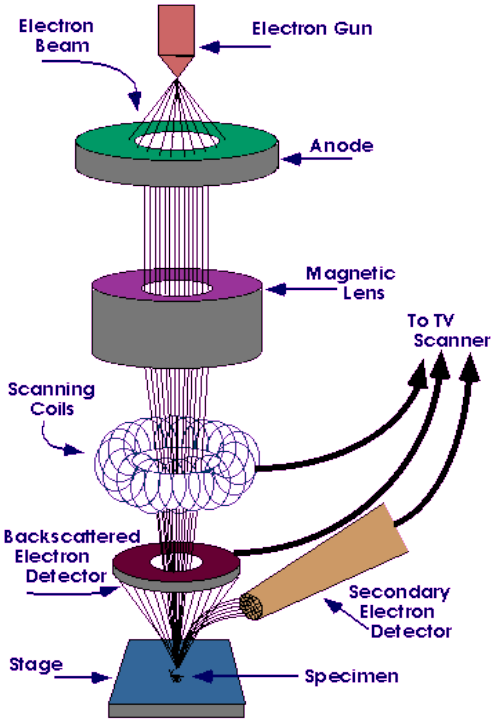

Figure 6: Components of a Scanning Electron Microscope. Obtained from (31).

Principles of Energy Dispersive Spectroscopy (EDS)

With EDS, the energy levels of the emitted x-ray photons are characteristic of the chemical elements in the excited sample. The emitted x-ray photons are counted electronically and categorized at each energy level as seen in *Figure 7*. Information about the chemical elements present in the sample is determined by x-ray photon counts at the characteristic spectral energy peaks of the elements. Additionally, the x-ray photon counts in the characteristic spectral peaks in relation to background counts provide a means to determine the percent of the element present in the mass excited by the electron beam (*Figure 8).* Finally, because x-rays are emitted as the electron beam scans over the specimen, the location of the characteristic x-rays emitted may be mapped in relation to the secondary electron image as seen in *Figure 9*.

There are several variables that affect the emitted x-ray signal. These variables include the energy of the electron beam exciting the specimen (expressed as kilovolts), the distance of the specimen from the pole piece of the magnetic lens (working distance,

WD), the spot size of the focused electron beam (diameter in nm), and magnification (15, 17).

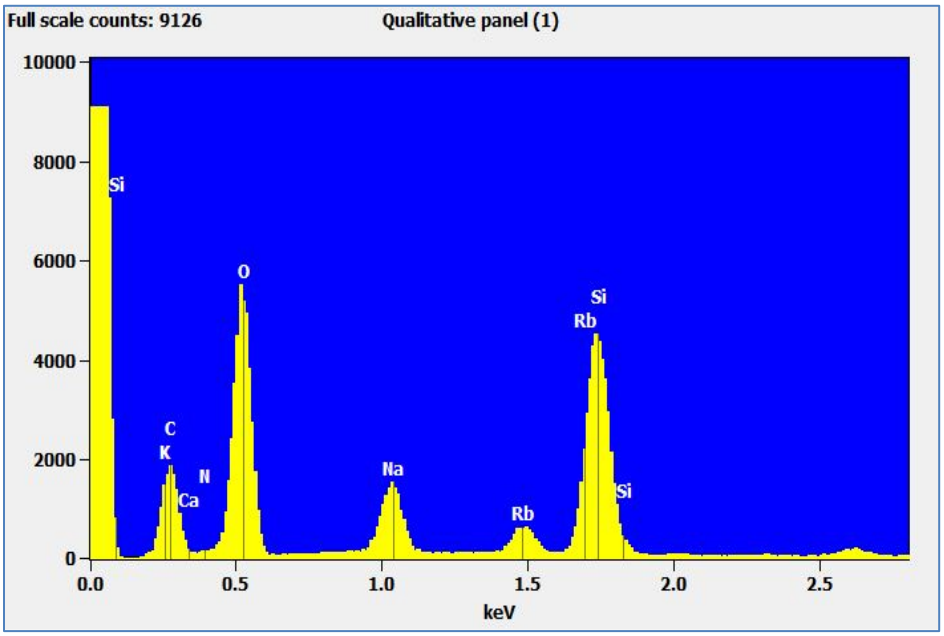

Figure 7: Spectrum showing x-ray photon emission from elements at energy levels between 0.0 kV and 3.0 kV on the x-axis, and 0 to 10,000 counts of x-ray on the y-axis. The area beneath each peak is used to determine the elemental weight percent.

Element Setup | Analysis Setup | Compare Information | Quant Results | Processing

Tue Feb 23 16:37:43 2016
Filter Fit Chi² value: 583.503
Correction Method: Proza (Phi-Rho-Z)
Acc.Voltage: 20.0 kV Take Off Angle: 39.3°

Element Line	Element Wt.%		Wt.% Error
C K	11.44	±	0.54
N K	27.93	±	0.75
O K	51.58	±	0.43
Na K	6.55	±	0.09
Si L	0.00	±	0.00
Si K	---		---
K L	---		---
K K	1.27	±	0.02
Ca L	---		---
Ca K	0.01	±	0.01
Rb L	1.22	±	0.50
Rb K	---		---

Total	100.00		

Figure 8: Report generated by Noran System Seven EDS software.

The software used in this study to interpret the x-ray emission is Noran System Seven (NSS), which allows elements to be selected for quantitative analysis. The relative

weights of elements present in the specimen are expressed as weight percent (% Wt). This value represents the weight of elements present in the tissue excited by the electron beam. In this study, the main elements present in samples were rubidium, sodium, potassium, calcium, chlorine, carbon, nitrogen, oxygen, and silicon. As previously discussed, rubidium is a potassium congener and was used in this study to determine sodium potassium pump activity. Sodium, potassium, calcium and chlorine were present extracellularly as part of residual Krebs buffer remaining with the incubated cells. These elements also appear intracellularly based on their biological functions within viable cardiomyocytes (26). Carbon, nitrogen and oxygen make up the majority cellular molecules (2). Finally, silicon is the primary component of the coverslips on which the samples were prepared and analyzed by SEM and EDS (9).

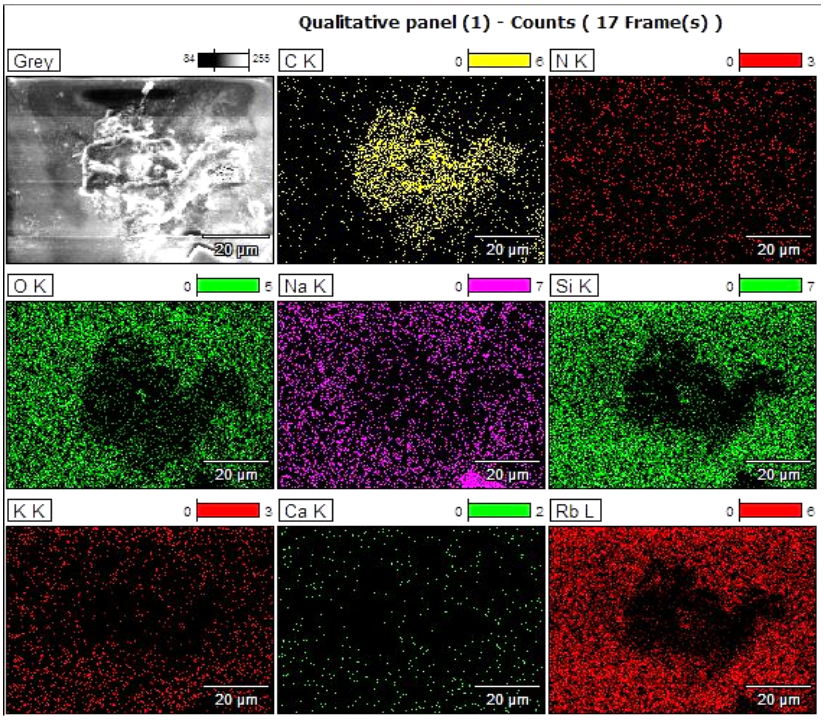

Figure 9: Map of elemental density in a sample. The spatial density of the dots indicates the number of x-ray photons emitted for each of the elements. Elements are indicated on the top left-hand corner of each panel and a gray scale SEM image is displayed in the top left corner panel.

In viable cells, elements such as calcium, potassium, and sodium make up an approximate 4% of the cell mass. Water makes up an approximate 70% of the cell mass, and macromolecules composed of carbon, oxygen, nitrogen, and hydrogen make up approximately 30% (2). It is important to note that cells analyzed on the SEM are dehydrated as part of their preparation, which means that the values expressed in this study represent percentage of specimen dry weight. Furthermore, because of instrument limitations, quantitative information for hydrogen cannot be obtained EDS. Thus, with practically no water remaining in freeze-dried dehydrated cells, elemental composition is distorted. Carbon and nitrogen make up anywhere between 60-70%, and the remaining elements make up the rest.

Data gathered are illustrated in a variety of useful modes. One such mode is a spectrum graph of the analysis as seen in *Figure 7*. The spectrum shows the x-ray energy levels (KeV) on the X-axis and x-ray photon counts at each energy level on the Y-axis. Each element emits x-ray photons at specific KeV energy levels depending on the electron orbitals (K, L, M) of the element. The amount of each element present in the sample can then be derived from the areas under the curve of the characteristic peaks and is expressed as weight percent. NSS also allows for manually focusing on a region of interest on the SEM specimen. Quantitative data gathered by the EDS at the specified area of interest is reported as weight-% as shown in *Figure 8*.

Materials and Methods

Experimental Design

To examine the inhibitory effects of linoleic acid on sodium pumps, viable cardiomyocytes were isolated from rat hearts and incubated in various buffers. Since rubidium was a close congener of potassium, it was used as index for potassium uptake by isolated rat cardiomyocytes. Rubidium was measured by using EDS technology as weight percent within a cell. Rubidium weight percent of cells incubating in rubidium-Krebs buffer was used as the experimental negative control expressing a baseline incorporation of rubidium in viable cardiomyocytes. Rubidium weight percent of cells incubating in Ouabain + rubidium-Krebs buffer was used as the experimental positive control expressing decreased incorporation of rubidium in viable cardiomyocytes due to Ouabain's inhibitory effect on sodium pumps. Linoleic acid's effect on sodium pumps was examined by incubating viable rat cardiomyocytes in L.A + Rubidium-Krebs buffer and then measuring rubidium weight percent of those cells by EDS.

Rats

The use of rats for this study was approved by the Institutional Animal Care and Use Committee at Minnesota State University, Mankato (IACUC approval # 15-04). Thirty Wistar-Kyoto (WKY) rats were used for the trial sets of this project. To maintain consistency, only adult males were used for the experiments. The weight range for the rats was between 260 and 320 grams. The rats were housed in the Animal Care Facility in Minnesota State University, Mankato and were fed standard commercial chow and water ad lib. The rats were housed in 1600cm^3 cages with wood chip bedding. Two rats were housed in each cage and the cages were in a room with a temperature set at 72° F and a 12-hour light/dark cycle.

Rat Heart Isolation

The first step of the experimental procedures was to remove rat hearts for cardiomyocytes isolation. In preparation for removal, the rats were anesthetized using 3% Isoflurane in oxygen gas administered to the rats through a gas chamber. After approximately 5-7 minutes of the Isoflurane gas administration, the rats were completely anesthetized. The Isoflurane gas was then shifted from the gas chamber into an anesthesia mask, in which the muzzle of a rat was fully inserted. The rats were laid in a ventral view on a surgical pad.

The heart was then removed by opening the thoracic cavity through a transverse incision below the sternum and bilateral parasagittal cuts through the ventral thoracic wall. Once apparent, the attachment of the diaphragm was incised to expose the heart. The aorta was then identified and cut one centimeter away from heart. The heart was then excised from the pericardium and separated from the lungs. The isolated heart was placed in a beaker containing approximately 30ml of 0.9% saline cooled to 4^{o} C to stop the heart-beat and allow for placement of a 16-gauge cannula in the aorta. The tip of the cannula was advanced retrograde to the ostia of the coronary arteries and the cannula was secured in place with a ligature.

Langendorff Apparatus and Administration of Digestive enzymes

The Langendorff system has a water-jacketed reservoir, infusion line, and organ chamber to maintain a constant temperature of infusate. The reservoir is located approximately 70 cm above the organ chamber to maintain a constant infusion pressure at around 52 mmHg. A sintered glass bubbler in the reservoir provides a means to deliver and saturate the infusate with oxygen gas. The Langendorff system allows for the perfusion of buffers containing tissue digestive enzymes. The digestive enzyme

collagenase type II (Worthington Biochemical Corp., Lakewood NJ) was used to break-up collagen within cardiac tissue and separate cardiomyocytes. To prepare the collagenase solution, 60 ml of calcium-free Krebs solution was heated to 37^0C, and 0.060g of the collagenase was dissolved in the 37^0C calcium-free Krebs solution.

Once the heart was cannulated and connected to the Langendorff apparatus, an infusion of 50 ml of normal Krebs buffer solution warmed to 37^0C was infused through the cannulated heart to initiate the heartbeat. During the infusion, the heart blanched from a red to a pale pink coloration and continued to beat. After infusion with the initial buffer solution, 25 ml of the collagenase-Krebs buffer was delivered to the heart through the Langendorff system for approximately 10 minutes. Following the infusion of collagenase-Krebs solution, the heart was disconnected from the Langendorff apparatus and the cannula was removed. The heart tissue was then minced into approximate $3mm^3$ pieces and incubated at 37^oC in a petri dish filled with collagenase in calcium-free Krebs solution. The incubation period lasted 30 minutes on a dissection warming-plate set at 37^0C.

Table 1: Krebs Buffer Solutions

Buffer	**pH**	**Composition**
Standard Krebs	7.35	5 mM KCl, 2 mM $CaCl_2$, 24 mM $NaHCO_3$, 1mM $MgCl_2$, 115 mM NaCl, 10 mM HEPES, BSA and ddH_2O
Calcium-Free Krebs	7.35	Standard Krebs. Eliminated $CaCl_2$, and adjusted pH to 7.35
Rubidium-Krebs	7.35	Standard Krebs. KCl is substituted with RbCl and adjusted pH to 7.35
Ouabain+ Rubidium-Krebs	7.35	Rubidium-Krebs + 10^{-3}M Ouabain, and adjusted pH to 7.35
Linoleic Acid+ Rubidium-Krebs	7.35	Two different concentrations of Linoleic Acid (10^{-3}M and 10^{-6}M) dissolved in Rubidium-Krebs, and adjusted pH to 7.35

Cardiomyocytes Isolation (Figure 10)

After incubation in collagenase-Krebs buffer, the isolated cells in the buffer were pipetted into two 15-ml Falcon tubes, using disposable 3 ml pipettes. The two falcon tubes were centrifuged at 700 x g for 1 minute. The supernatant containing the collagenase solution was decanted. The remaining pellets containing the isolated cardiomyocytes were washed twice in calcium free Krebs to wash off residual collagenase and to ensure the termination of digestive enzyme activity. Each wash consisted of adding 2 ml of 37^0C calcium-free Krebs solution to each of the two falcon tubes. The cell pellets were then resuspended into solution and centrifuged at 700 x g for 1 minute. Following the two washes, 1 ml of 37^0C rubidium-Krebs solution was added to each of the two pellets, and the cells were resuspended in the solution. Rubidium Krebs is a variant of the buffer where potassium is completely replaced with rubidium. The two falcon tubes were combined into a single tube resulting in a 2 ml cardiomyocyte cell suspension. The suspension was maintained at 37^0C at all times on a heating platform. All buffer solutions used in this experiment were preheated to 37^0C using a heating platform, and oxygenated using the scintered glass oxygen gas bubbler.

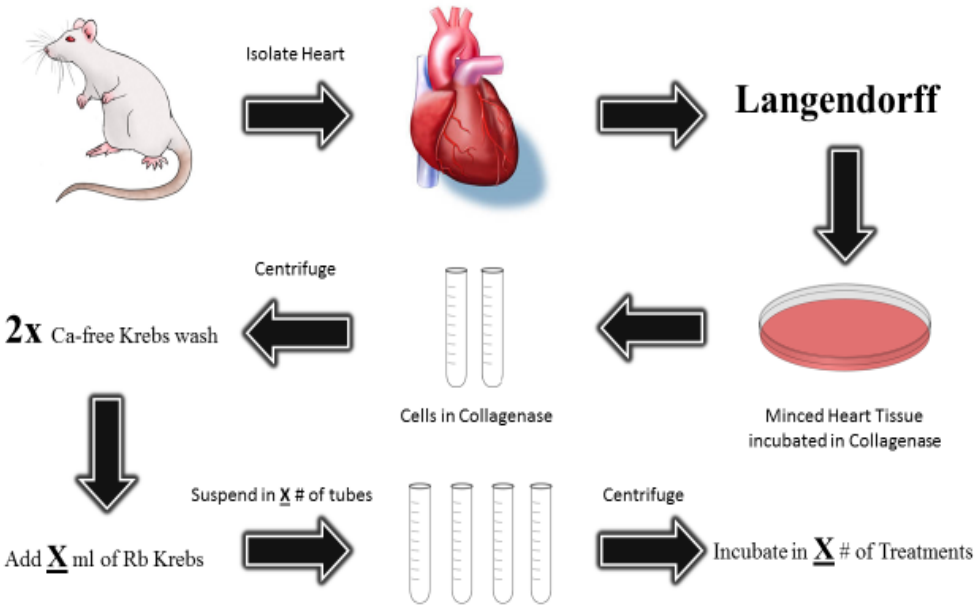

Figure 10: Cardiomyocyte isolation procedure.

Trypan Blue

A Trypan Blue assay was conducted to confirm the viability of the isolated cells. This assay was used when there was a procedural change and when new batches of buffer or collagenase stock were being used to confirm proper cardiomyocyte isolation. To prepare the Trypan solution, 0.4 g of lyophilized Trypan were dissolved in 100 ml phosphate buffered saline (PBS) solution by slow-boil. The solution was let to cool to room temperature, and then stored in a 10^0C refrigerator. To conduct the assay, 5µl of the Trypan solution were gently mixed with 45µl of the cardiomyocyte cell-suspension. Incubation was continued at 37^oC on the remaining cell suspension. The Trypan blue/cell suspension assay mixture was incubated for 5 minutes at 37^0C.

After the incubation period, the assay mixture was gently remixed using a micropipette, and then 20 µl were pipetted and dispensed on a slide. A coverslip was then gently applied onto the sample. The slide was observed on a Zeiss light-compound microscope at a total magnification of 400x. The trypan blue dye works as an exclusion assay, since viable cells with intact cellular membrane exclude the dye and remain unstained. Conversely, dead cells incorporate the dye and appear distinctly stained blue when viewed under a light compound microscope. The slide was observed in its entirety, and ratio of live-to-dead cells was determined.

Contractility Studies

Contractility studies were done in order to examine the ability of isolated cardiomyocytes to function properly. The studies were an attempt to induce contractions of isolated cardiomyocytes to further confirm their viability. A 0.5ml sample of the cardiomyocyte cell-suspension was placed in a contractility apparatus *(Figure 11*). The apparatus consisted of a cell culture well with both a positive electrode and a negative electrode properly secured at opposite ends of the well. The electrodes were connected to

a power source supplying pulsed voltage with the parameters detailed in *Table 2*. The contractility apparatus including the 0.5ml of cardiomyocytes isolate was placed on an inverted microscope and was viewed at total magnification of 400x. Since cardiomyocytes function best around 37^0C, the temperature of the well placed on the microscope was recorded for duration of 15 mins in 5 mins increments as seen in *Table 3*. To overcome the drop in temperature inside the contractility well, the well was placed inside a petri dish filled with 40^0C distilled water. The power supply conditions were also manipulated in an attempt to induce contractions.

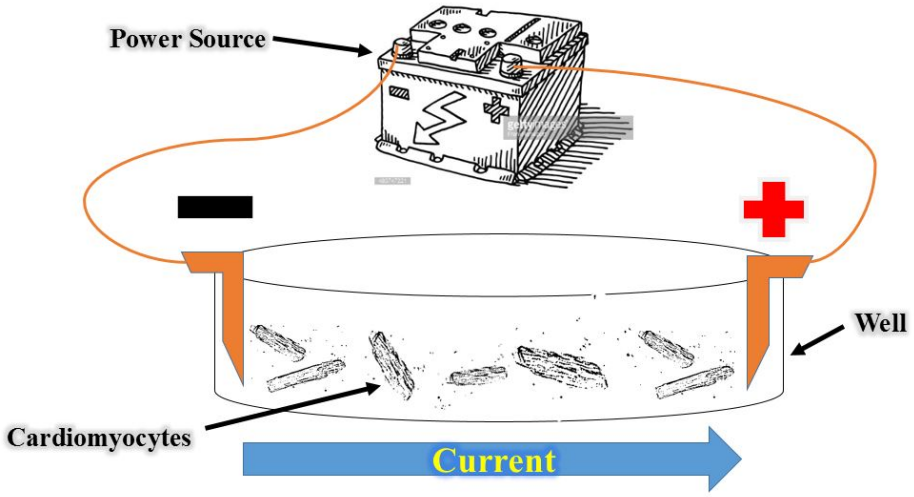

Figure 11: Diagram illustrating contractility studies.

Table 2: Power supply	
Frequency	5 pulses per second
Delay	2 millisecond
Duration	2 millisecond
Voltage	0.1 Volts

Table 3: Temperature of	
Time (mins)	Temperature (^{0}C)
0	37
5	26
10	23
15	23

Cell Adhesion onto Coverslips

An investigative step was conducted to estimate the time needed for a cell to precipitate out of the saline preparation, and settle onto the coverslip. Samples of isolated cardiomyocytes in 1 ml of 0.9% saline were observed under a light compound microscope. The microscope was first adjusted in fine focus onto a slide at total magnification of 400x. Then a drop of the cell isolate was placed onto the slide in focus. Time was determined from placement of drop until cells settled on the surface of slide in focal plane. The time for the cells to settle was approximately 20-30 sec. Subsequently, 1.5 min after placement of the suspension on the coverslip, the solution was perturbed using a P-20 pipette to determine whether the cardiomyocytes had settled completely onto the coverslip.

SEM/EDS Sample Preparations

After incubation in treatment buffers, cardiomyocyte samples were washed twice in 0.9% saline solution. The wash consisted of centrifugation of cells incubated in treatment buffers at 700 x g for 1 minute, the supernatant was then decanted. The pellet of cells was resuspended in 1 ml of 0.9% saline solution, and centrifuged at 700 x g for 1 minute, and the process was repeated for the second wash. Following the two washes, the cells were suspended in 0.25 ml of 0.9% saline solution. To freeze-dry the samples, 0.25 ml of each cell preparation were dispensed evenly on two coverslips for a given treatment. The coverslips were submerged for10 seconds in liquid nitrogen, and immediately placed on the cold plate of a *VirTis 4KB Benchtop* freeze drying apparatus pre-set at -60^{0} C. The samples were freeze-dried at 095mTorr for 12 hours.

SEM/EDS Procedure

The scanning electron microscope JEOL JSM 6510LV (JEOL U.S.A, Inc.) equipped with a Thermo NORAN silicon drift ultra-dry detector, EDS system, and NSS system-7 analysis software (Thermo Scientific) was used to analyze the elemental content of the samples. The samples were not sputter coated with conductive material (i.e. gold) minimize potential interference in EDS analysis.

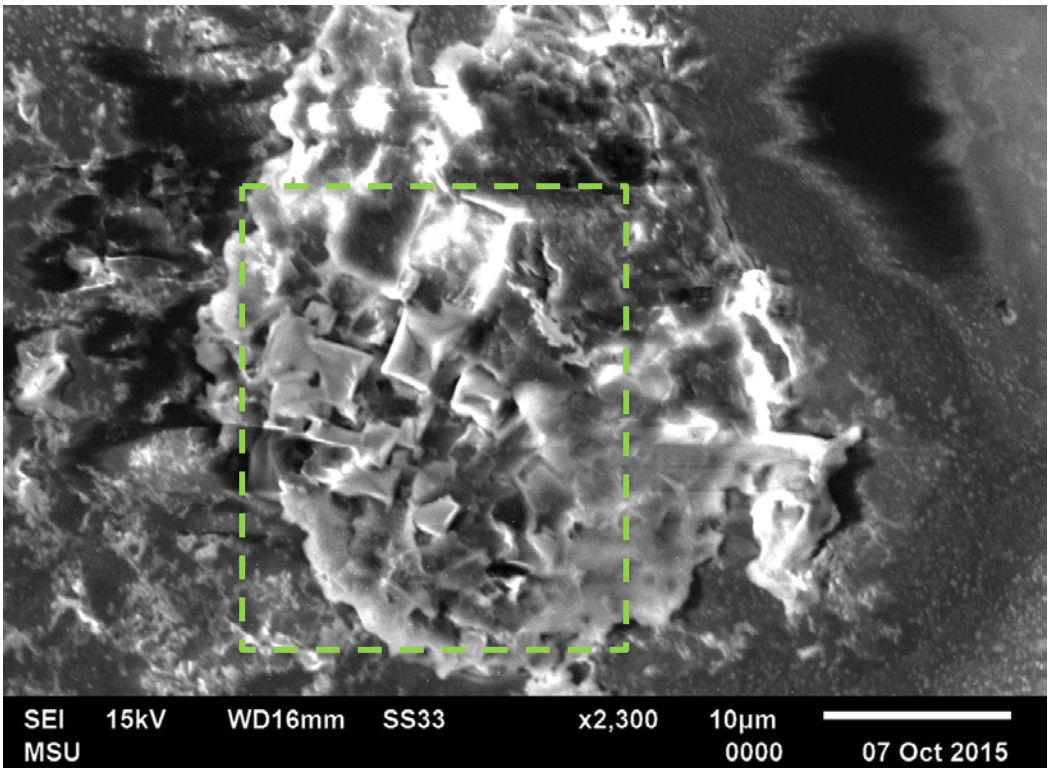

Figure 13: An SEM of an isolated cardiomyocyte not accepted for EDS analysis. This cell was rejected from analysis because it was heavily covered in salts. Sharp-edged salts could be seen inside the region highlighted by the dashed green box x2,300.

For EDS analysis, samples were analyzed at 8000X so that the cell encompassed the entirety of the field of view. Samples were analyzed with an accelerating voltage of 20 kV, with a spot size of 50 nm. These parameters were decided based on preliminary trials for optimal detection of rubidium at different spot sizes and kV levels (*Appendix B* and *Appendix C*). A cell was selected for EDS analysis if it was fully-intact and flattened, not folded, on the surface of the coverslip. Furthermore, each of the analyzed cells was free

of salts or other debris within the entirety of the cell's surface. Cells with salt crystals embedded on the surface (*Figure 12*) were not selected for analysis due to inaccurate results caused by salt crystals and debris. Analysis was conducted to detect element weight % for sodium (Na^+), carbon (C), nitrogen (N), oxygen (O), potassium (K), calcium (Ca), silicon (Si), and rubidium (Rb). These elements had characteristic x-ray photon energy peaks between 0 and 3.0 KeV, and a 5-minute scan yielded x-ray counts between 0 and 10,000 at characteristic energies. The main peaks were observed for sodium (Na^+) at 1.04 KeV, for carbon (C) at 0.27 KeV, for nitrogen (N) at 0.39 KeV, for oxygen (O) at 0.52 KeV, for potassium (K) at 3.31 KeV, for calcium (Ca) at 0.34 KeV, for silicon (Si) at 1.73 KeV, and for rubidium (Rb) at 1.69 KeV. Reports generated for the samples included a quantitative report, mapping of elements, and spectrum readings.

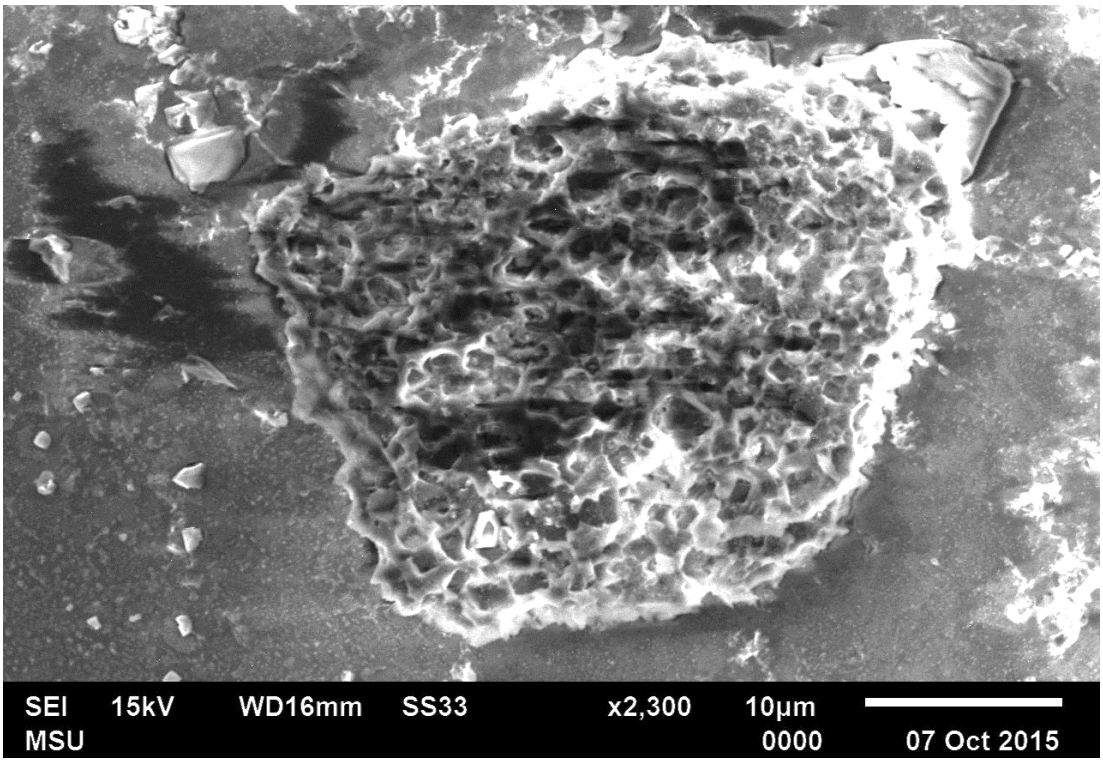

Figure 13: SEM of an isolated cardiomyocyte accepted for EDS analysis during the preliminary phase of the study. This cell is viewed at a magnification of x2,300, 15kV, and a spot size of 33nm.

The above procedure was used in preliminary trials to determine optimal conditions for analysis and to examine linoleic acid's effects on cardiomyocyte rubidium levels. The preliminary trials included optimal time for rubidium uptake, optimal electron beam spot size, optimal electron beam accelerating voltage, and confirmation of optimal Ouabain concentration to induce inhibition of rubidium uptake. The methodology and results of the preliminary trials are included in *Appendices A-E.*

The Effects of Linoleic Acid on Cardiomyocyte Rubidium

Based on the preliminary trials (*Appendices A-E),* the experimental procedure and analytical conditions were set to examine the proposed hypothesis in ten replicates. Each experimental replicate included cells incubating in Rb-Krebs buffer (negative control), 10^{-3} M Ouabain + Rb-Krebs buffer (positive control), 10^{-3} M L.A+ Rb-Krebs buffer, and 10^{-6} M L.A+ Rb-Krebs buffer. All cells for one experimental replicate were isolated from one rat heart (Figure 10) and divided equally between the four treatment buffers. Cells in each treatment incubated for two hours, which was determined to be optimal incubation period as seen in *Appendix A.* For each experimental treatment, 10 cells were randomly selected for analysis. Parameters for SEM/EDS analysis were decided based on the results of preliminary trials (Appendix B and C). As previously mentioned, cells in all ten experimental replicates were analyzed at a magnification of x8000, a spot size of 50 nm, and a voltage of 20 kV.

Statistical Analysis

Microsoft Excel data for each experimental trial was transferred to Statistical Package for Social Sciences (SPSS) software. The data groups were analyzed for normal distribution using the Wilk-Shapiro test with p-value greater than 0.05 considered

normally distributed. Levene's test for equality of variance was conducted under the assumption that variance of data in treatment groups were not equal. Variances were considered equal if p-values were greater than 0.05. Analysis of Variance (ANOVA) test was conducted for experimental groups to determine if there were statistically significant differences among the means of treatment groups. An ANOVA P-values less than 0.05 indicated that there was a significant difference among treatment groups. If significant differences were found, then Tukey's post-hoc test was conducted to determine where the significance lies among the groups. Differences identified by the Tukey post-hoc test were considered to be significant if p was less than 0.05.

Results

Viability of Cells

Observed cardiomyocytes appeared to be rectangular in shape and had an approximate area between 900µm^2 and 1650µm ^{2} as seen in *Figure 13*. Cardiomyocytes were examined for viability using a Trypan Blue exclusion test. This process was performed when there was a change in procedure or when a new batch of buffer and collagenase were used. As shown in *Figure 14*, some cells incorporated the dye, and thus were considered dead, while other cells did not incorporate the dye, and therefore were considered viable. Preparations of isolated cells producing a ratio as low as one-to-one live-to dead cells were considered an acceptable batch for subsequent incubation in treatment and analysis.

Contractility studies were also conducted. However, cardiomyocyte contractions were not observed and the cardiomyocytes appeared to be in a hyper-contracted state as described by Dalen et al (6). The surface of the cells had a shriveled appearance that was highly wrinkled. Often small blebs protruded from the surface of the cells and were probably mitochondria squeezed towards the cell surface (6). Furthermore, the appearance of isolated cardiomyocytes in this study may have been distorted because of the freeze-drying procedure.

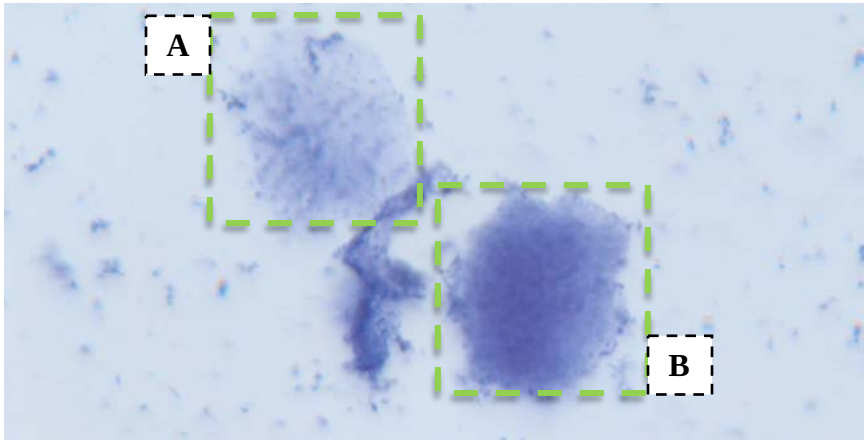

Figure 14: Image showing **A)** a viable cardiomyocyte, and **B)** a dead cardiomyocyte Magnification x400.

The Effects of Linoleic Acid on Cardiomyocyte Rubidium

The main question of this thesis study was "how would linoleic acid effect rubidium uptake in isolated rat cardiomyocytes?" Table *4* shows the mean weight percent of rubidium for each of the four treatment groups in ten replicates. In each of the ten trials, the rubidium levels were measured in ten cardiomyocytes for each of the treatment groups. Raw data for each experimental replicate are listed in *Appendix F*. The mean and standard errors for each treatment are expressed numerically at the bottom of *Table 4* and graphically in *Figure 15*.

Table 4: The Effects of Linoleic Acid and Ouabain on Cardiomyocyte Rubidium

	Mean Rb Weight Percent per Replicate for different Treatments			
Replicate	**Rb Krebs Without Treatment**	**10^{-6} M Linoleic Acid +Rb Krebs**	**10^{-3} M Linoleic Acid +Rb Krebs**	**Ouabain (10^{-3} M) +Rb Krebs**
1	**1.089** ± 0.206	**1.264** ± 0.303	**1.445** ± 0.329	**1.024 ±** 0.132
2	**2.096** ± 0.177	**0.461** ± 0.140	**0.528** ± 0.191	**0.729** ± 0.165
3	**1.474** ± 0.153	**0.425** ± 0.199	**1.166** ± 0.222	**0.629** ± 0.113
4	**1.088** ± 0.239	**0.521** ± 0.233	**0.683** ± 0.254	**0.569** ± 0.195
5	**0.863** ± 0.270	**1.536** ± 0.211	**--**	**0.679** ± 0.214
6	**1.152** ± 0.153	**1.097** ± 0.338	**0.710** ± 0.230	**0.29** ± 0.140
7	**1.312** ± 0.145	**0.886** ± 0.128	**0.92** ± 0.337	**0.586** ± 0.232
8	**1.082** ± 0.174	**0.444** ± 0.210	**0.92** ± 0.224	**0.732** ± 0.223
9	**1.236** ± 0.193	**0.675** ± 0.184	**0.701** ± 0.171	**1.123** ± 0.218
10	**1.399** ± 0.219	**0.749** ± 0.189	**1.059** ± 0.203	**0.654** ± 0.213
Average	**1.279** ± 0.075	**0.805** ± 0.121	**0.903** ± 0.095	**0.701** ± 0.073

For average rubidium weight percent per replicate, cells incubated in “Rb-Krebs without treatment” resulted in a mean of 1.279 +/- 0.075, and a Wilk-Shapiro normal distribution p-value of 0.061. Cells incubated in 10^{-3} M L.A. resulted in a mean rubidium weight percent of 0.903 +/- 0.095, and Wilk-Shapiro normal distribution p-value of 0.652. It is important to note that the L.A. concentration of 10^{-3} M had only nine replicates, whilst all other treatments had ten. The missing replicate was a trial that failed to produce ten acceptable cells; thus the trial was considered inadequate for analysis. Cells incubated in 10^{-6} M L.A resulted in a mean rubidium weight percent of 0.805 +/- 0.121, and Wilk-Shapiro normal distribution p-value of 0.193. Cells incubated in “Ouabain + Rb-Krebs” resulted in a rubidium weight percent mean of 0.701 +/- 0.073, and Wilk-Shapiro normal distribution p-value of 0.349. All treatment groups were considered to have a normal distribution of values. Levene’s test for equality of variance yielded a p-value of 0.382, which indicates that variances within treatment groups are equal amongst all groups. A one-way ANOVA resulted in a p-value of 0.002, indicating a significant difference among groups. The Tukey post-hoc multiple comparison test indicated that cells incubated in both treatment groups “Ouabain + Rb-Krebs” (p-value=0.001), and “10^{-6} M L.A” (p-value=0.010) had statistically significant lower average rubidium weight percent values compared to cells incubated in “Rb-Krebs”. There was no statically significant difference between the treatment groups “10^{-3} M L.A” (p-value=0.64) and “Rb-Krebs”. Also, there were no statistically significant difference amongst the treatment groups “10^{-3} M L.A”, “10^{-6} M L.A”, and “Ouabain + Rb-Krebs” (All p-values > 0.05).

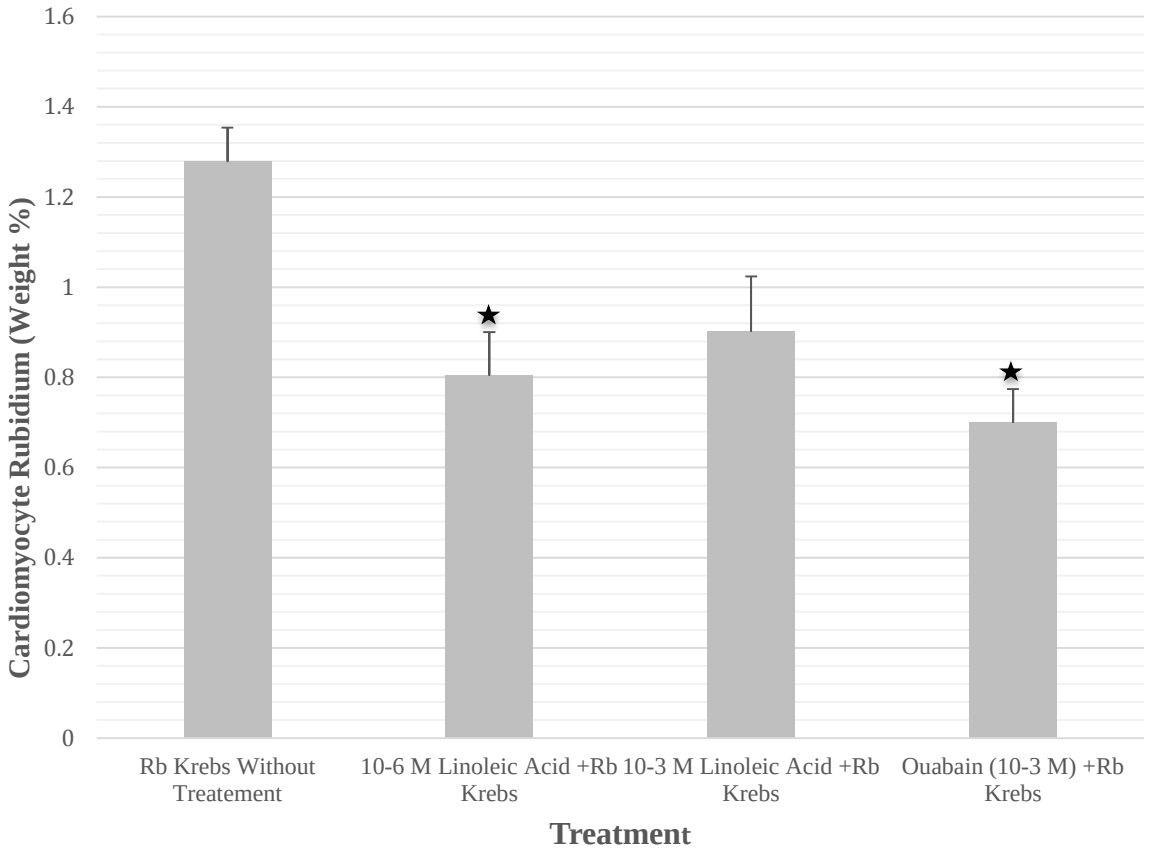

Figure 15: Mean cardiomyocyte rubidium weight percent. Error bars represent Standard Error. Stars indicate significant difference from "Rb Krebs without Treatment" ($P<0.05$).

Discussion

This study was designed to examine the potential of linoleic acid as an inhibitor of sodium potassium pump activity. This was done by measuring rat cardiomyocyte rubidium levels using EDS. It was found that the linoleic acid concentration 10^{-6} M, and not 10^{-3} M, exhibited an inhibitory effect on rubidium uptake. Several studies have shown that linoleic acid metabolites are incorporated into the phospholipids of cellular membrane in a manner that can alter the functions of cellular membranes (12, 32). Ha et al. proposed that linoleic acid molecules interject within the cellular membrane in regions close to sodium potassium pumps, and that disrupts the cellular membrane fluidity and the sodium pump function in the process (12). One potential explanation for the lack of inhibitory effect by the higher concentration of linoleic acid, 10^{-3} M, is increased non-specific lipid interactions caused by the hydrophobic nature of linoleic acid, which may alter and counter the inhibitory effect otherwise observed with the lower linoleic acid concentration at 10^{-6} M. Secondly, downregulation or upregulation of transmembrane enzymes involved in ion movement across cellular membranes could be another potential explanation. Linoleic acid was shown to downregulate the expression of specific enzymes, such as desaturase, at a transcriptional level by acting on sterol regulatory element binding protein (SREBPs) (32). Thirdly, linoleic acid was shown to have several physiological effects both through one of its isomers or as a precursor of a biologically active compound (30). For example, linoleic is a precursor of prostaglandins through the intermediate arachidonic acid (30). Prostaglandins are a biologically active lipid compounds with hormone-like effects, and so perhaps at increased concentrations, linoleic acid may affect cellular element concentration differently-than at lower concentrations- though hormone like interactions. Finally, the lack of observed inhibition by 10^{-3} M linoleic acid concentration could be due to a statistical artifact. Statistically, the

treatment 10^{-3} M had a smaller sample size, compared to the other treatment groups, as no sufficient data was obtained from the 10^{-3} M within trial set 5 (*Appendix F*).

Cardiomyocyte viability

The viability of isolated cardiomyocytes was confirmed by the trypan blue assays whenever a new stock of buffers was used or to confirm a change in cardiomyocyte isolation methodology. It is important to note that with the trypan blue assays, a ratio as low as one-to-one live-to-dead cells was accepted. This, of course, introduces the chance that some of the cells analyzed might have been dead cells. In addition, no confirmation of cell viability was conducted following the 2-hour incubations, which could also mean that decreased cardiomyocyte rubidium levels observed in cells treated with Ouabain and linoleic acid were a result of cell death caused by Ouabain or linoleic acid. To better understand the results produced in this thesis, it would be important to examine the effect of cellular death on rubidium incorporation. It would also be worthy of considerations to confirm the viability of cells post-incubation in the various treatment buffers.

To further confirm the viability of isolated cardiomyocytes, examination of cardiomyocyte contractility was conducted. The aim was to demonstrate that these isolated cardiomyocytes were not only viable, but they were also functioning. However, the contractility of the cardiomyocytes could not be demonstrated in this thesis. The most likely explanation for lack of contractility is that the cells appeared to be hypercontracted state with similar morphology to what Dalen et al. described (6). In fact, adult cardiomyocytes, such as the ones isolated in this study, are difficult to induce in-vitro contractility and that neonatal cells are preferred amongst researchers due to their ability to contract in-vitro (3).

Cellular Rubidium Levels

The cellular levels of rubidium were most likely a result of the sodium potassium pump transport. There is a chance, however, that rubidium was incorporated into cardiomyocytes through other cellular membrane channels or pumps. Previous work has indicated that rubidium is actively transported into cells through sodium potassium pumps (4,18, 21). In this thesis, Ouabain, a known inhibitor of the sodium potassium pump, reduced cardiomyocyte rubidium levels, providing evidence for cellular uptake of rubidium through sodium potassium pumps. The rubidium levels inside the cell boundaries were less than the levels outside the cell boundaries as seen in *Figure 16*, qualitatively, and *Figure 17*, quantitatively. This indicates that perhaps the cellular membranes were functioning as a selective barrier against rubidium. The external environment of the cells was composed of residual Rb-Krebs salts and saline. Finally, to examine whether rubidium detected was on the surface of cells or inside the cells, a preliminary study was conducted using different accelerating voltages of the electron beam. With voltage increases, the electron beam penetrates deeper into the sample (appendix C). There was a drop in rubidium levels detected at voltage levels of 25 and 30 kV where the electron completely penetrated through the sample. At 15 kV, the electron beam penetration was not as deep and the EDS detected moderate levels of rubidium. And at 20 kV, the electron beam went deeper into cells and detected significantly higher levels of rubidium as seen in *Appendix C.* This indicates that at the 20 kV level, the electron beam wasn't deep enough to over-shoot cells and not shallow to pick surface rubidium. Instead, at 20 kV the EDS detected rubidium incorporated inside isolated cells.

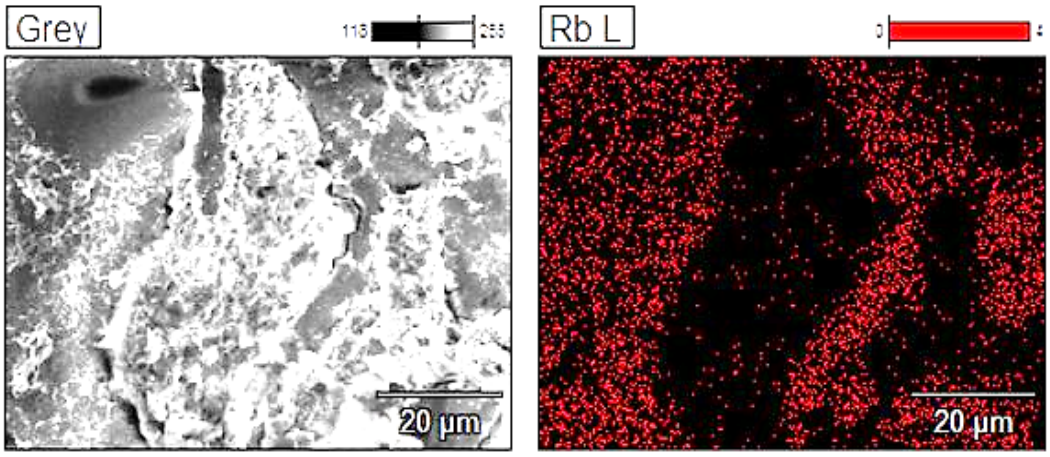

Figure 16: Scanning electron micrograph of cardiomyocyte and its immediate surroundings (left) with corresponding map of rubidium (right). x1,600.

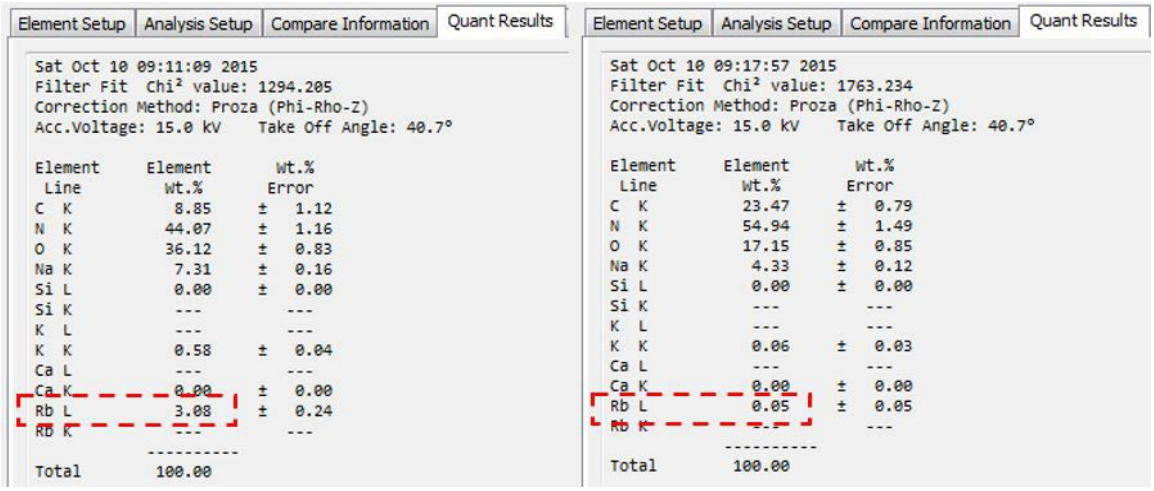

Figure 17: Elemental composition of the areas scanned in *Figure 16*. Left panel lists weight percent of elements outside the cell boundary. Right panel lists weight percent of elements inside the cell boundary. x8,000.

There was a significant concern regarding the close proximity of silicon and rubidium peaks on the EDS spectrum as seen in *Figure 7*. Silicon, the main component of the coverslips on which cells were prepared, has a peak at 1.73 kV on the spectrum whereas rubidium has a peak at 1.69 kV on the spectrum. The proximity of the peaks raised a concern that the silicon from the coverslip interfered with rubidium measurement. To understand the degree of interference by silicon, the rubidium levels from cells prepared on a graphite, or carbon, support were compared to those mounted on

a silicon coverslip (*Appendix E*). The results indicated that primary element detected was rubidium and not silicon. However, use of carbon support in the main experiment made it impossible to detect cellular carbon, which was an indicator for accepting cells for SEM/EDS analysis. As previously mentioned the element carbon makes up a large portion of dried cells, and carbon stubs as a background to isolated cells distorts carbon element weight percentages detected by EDS. It is also important to note that throughout the entire study, the percentage of silicon remained consistent and did not vary with treatment. This was especially the case when cells were analyzed at 20 kV. Silicon-based coverslips were chosen as the surface to prepare samples only because of their consistent success in allowing intact cells to adhere to their surface throughout preparation process. Cells must also be able to settle out of solution and adhere on the surface of preparation before deep freezing in liquid nitrogen. Other surfaces such as aluminum and carbon specimen mounts and carbon tape did not provide an adequate surface for cell adhesion or for analysis

In the preliminary phase of this study, two biological phenomena were replicated. The heart cells in this study incorporated rubidium in a time dependent fashion similar to that reported by Kupriyanov et al (21). Cardiomyocyte rubidium in isolated cells over time was observed similarly in this study as seen in *Appendix A*. Furthermore, this study showed that treatment with Ouabain, a known inhibitor of the sodium potassium pump, reduced myocardial rubidium levels indicating that the observed cellular rubidium levels in this study were a result of the sodium potassium pump.

Limitations

It is important to note that there were several limitations to this study. Firstly, EDS technology is considered a semi-quantitative type of measurement since it only presents a percentage of the elements present in the cell and not the actual molecular composition of the cell (13). For instance, water comprising over 70% of the cell was removed by the dehydration process to prepare specimens. Secondly, the actual and physical depth of an isolated cardiomyocyte could not be measured nor could the depth of electron beam penetration of electron beam into the cell. However, the presence of silicon from the coverslip suggested that the beam penetrated through the cell exciting the elements within. Finally, the state of contracting versus relaxed cells was not known in the SEM/EDS analysis. However, from the observations of Dalen (6), the cardiomyocytes in the present study appeared to be in a hypercontracted state. This could have possibly effected the folding of a cell onto itself in a contracted state, which could alter elemental composition per unit area.

Future studies

Several experiments using the same experimental design of this study could be conducted to further understand the mechanism of inhibition exhibited by linoleic acid. One proposed experiment is to treat isolated cardiomyocytes with “Rb-Krebs + linoleic acid + Ouabain”, “Rb-Krebs + linoleic acid”, and “Rb-Krebs + Ouabain”. This experiment would show whether linoleic acid has an added effect of inhibition on top of the established effects of Ouabain. Rubidium weight percent within elements would be the experimental index for sodium pump inhibition as previously established. If the treatment group “Rb-Krebs + linoleic acid + Ouabain” was found to have decreased levels of rubidium compared to “Rb-Krebs + Ouabain”, then this indicates that inhibition

is perhaps observed through several pathways. The pathway of inhibition is of great significance to this study, since Ouabain's and digoxins competitive inhibition of potassium incorporation at the E2P conformation of sodium pumps results in the digitalis toxicity symptoms CHF patients' experience. A non-competitive inhibition through an allosteric site or an inhibition of sodium potassium pumps through disruption of cellular membrane offers an entirely new realm of possibilities for therapeutic specificity and regulation.

Also, the differential effect of linoleic acid concentration makes it crucial to examine other concentrations of linoleic acid. It is suggested for future studies that a dose dependent response is conducted using the same experimental design. This will further our understanding of linoleic acids effects on sodium potassium pumps, and will lead to the development of more solid ground for therapeutics. Furthermore, other fatty acids such as oleic acid and metabolites of linoleic acid should also be examined using this same experimental design. Other studies have shown that those metabolites of linoleic acid and other fatty acid exhibit biologically relevant effects on isolated cells (25, 32).

Several suggestions for future study were developed based on findings and course of research. It is suggested to utilize a single cardiomyocyte cell line from which treatments of linoleic acid and controls are applied. This will decrease the experimental steps preceding incubation in treatments, which in turn will reduce confounding variable including intrinsic differences in rats being used, and experimental and equipment errors in cardiomyocyte isolation steps. Such errors could significantly vary viability percentages of isolated cells, and it could also vary the fitness level of cells to exchange sodium and rubidium ions. This proposed cell line, however, could possibly introduce a new set of variable such as maintenance of cell line and potential bacterial infections.

To further confirm findings from this study, it is highly suggested that a detailed examination is conducted of potassium, sodium and calcium element weight percentages included in EDS (NSS) data sets obtained throughout the study. The aforementioned elements have biologically significant and independent correlations with rubidium uptake levels by isolated cardiomyocytes. Since the isolated cells were incubated in a potassium-free Krebs buffer, it is proposed that cells incorporating minimal levels of rubidium would contain higher levels of potassium. Potassium naturally *leaks* from inside the cell onto the extracellular matrix in efforts to maintain a balanced ionic gradient about the cellular membrane. If the sodium pump activity of cells incubating in rubidium is inhibited, 1) the cell wouldn't incorporate rubidium, and 2) leakage of intracellular potassium isn't favorable unless the cell is in a hypotonic state, and therefore potassium is retained inside the cell.

Sodium is the element directly exchanged for rubidium through sodium-potassium pump activity. It is hypothesized that as rubidium levels inside the cells decrease, through inhibition of sodium potassium pumps, an increase of intracellular sodium levels will be observed. With the concurrent experimental design, cells that completed incubation in treatment groups were washed in 0.9% saline, freeze-dried, and then analyzed on the SEM/EDS. This step causes an abundance of sodium molecules being detected by EDS throughout the sample preparation, since the cells are suspended in a sodium salt buffer. To analyze intracellular sodium levels, it is also suggested that the 0.9% saline solution is replaced with another solution such as concentrated glucose. A highly concentrated glucose solution would create a hypotonic environment for the cells, which would force the cells to retain their intracellular content in a fashion similar to the saline solution. This will result in more accurate EDS sodium readings since excess extracellular sodium will not interfere with the analysis. An observation of increasing

sodium levels as rubidium decreases inside cells is further confirmation of the inhibitory effects of linoleic acid.

Finally, calcium levels are a great indicator that indeed an inhibition of sodium pumps is occurring. It is hypothesized that in cardiomyocytes with decreased rubidium element weight percentages there will be a significant increase in intracellular levels. This is due to the aforementioned coupling of sodium potassium pumps and NCX activities. Increased intracellular levels of calcium is a promotor of more forceful cardiac contractions. The significance of such finding would further indicate the validity of utilizing linoleic acid as a treatment for congestive heart failure.

Work Cited

(1) Ahmad, A., Husain, A., Mujeeb, M., Khan, S. A., Najmi, A. K., Siddique, N. A, Anwar, F. (2013). A review on therapeutic potential of Nigella sativa: A miracle herb. *Asian Pacific Journal of Tropical Biomedicine, 3*(5), 337-352.

(2) Alberts, B. (2009). *Essential cell biology* (3rd ed.). New York: Garland Science.

(3) Aratyn-Schaus, Y., Pasqualini, F. S., Yuan, H., Mccain, M. L., Ye, G. J., Sheehy, S. P., Parker, K. K. (2016). Coupling primary and stem cell–derived cardiomyocytes in an in vitro model of cardiac cell therapy. *The Journal of General Physiology J Gen Physiol, 147*(3), 389-397.

(4) Beck, F. X., Dorge, A., Blumner, E., Giebisch, G., & Thurau, K. (1988). Cell rubidium uptake: A method for studying functional heterogeneity in the nephron. *Kidney International*, *33*(3), 642-651.

(5) Bell, R., Mocanu, M. & Yellon, D. (2011). Retrograde heart perfusion: The Langendorff technique of isolated heart perfusion. *Journal of Molecular and Cellular Cardiology* 50, 940-950.

(6) Dalen, H. (1998). *Effect of Collagenase on Surface Expression of Immunoreactive Fibronectin and Laminin in Freshly Isolated Cardiac Myocytes*. *Journal of Molecular and Cellular Cardiology, 30*(5), 947-955.

(7) Darling, R. A., Zhao, H., Kinch, D., Li, A., Simasko, S. M., & Ritter, S. (2014). Mercaptoacetate and fatty acids exert direct and antagonistic effects on nodose neurons via GPR40 fatty acid receptors. *AJP: Regulatory, Integrative and Comparative Physiology, 307*(1), 35-43.

(8) Felicilda Reynaldo, R. F. (2013). Cariac glycosides, digoxin toxicity, and the antidote. *CNE, 22*, 258- 261.

(9) Fisher Scientific (2016). *Fisherbrand™ Cover Glasses.* Obtained on 3-21-2016 from: https://www.fishersci.com/shop/products/fisherbrand-cover-glasses-squares-8/p-45512

(10) Fuller, W., Tulloch, L. B., Shattock, M. J., Calaghan, S. C., Howie, J., & Wypijewski, K. J. (2013). Regulation of the cardiac sodium pump. *Cellular and Molecular Life Sciences, 70*(8), 1357-1380.

(11) Go, A., Mozaffarian, D., & Roger, V. (2013). Executive Summary: Heart Disease and Stroke Statistics--2013 Update: A Report From the American Heart Association. *American Heart Association,* (127), 143-152.

(12) Ha, J., Dobretsov, M., Kurten, R. C., Grant, D. F., & Stimers, J. R. (2002). Effect of Linoleic Acid Metabolites on Na+/K+ Pump Current in N20.1 Oligodendrocytes: Role of Membrane Fluidity. *Toxicology and Applied Pharmacology*, 182(1), 76-83.

(13) Hafner, Bob (n.d). *Energy Dispersive Spectroscopy on the SEM: A Primer*. Characterization Facility, University of Minnesota- Twin Cities.

(14) Harvard University (2016). *K-level and L-level emission lines in KeV.* Obtained on 3-21-2016 from: http://www.med.harvard.edu/jpnm/physics/refs/xrayemis.html

(15) Hayat, M. A. (1978). *Introduction to biological scanning electron microscopy*. Baltimore: University Park Press, Part One, pp. 3-53.

(16) Heidenreich, P. A., Trogdon, J. G., Khavjou, O. A., Butler, J., Dracup, K., Ezekowitz, M. D., . . . Woo, Y. J. (2011). Forecasting the Future of Cardiovascular Disease in the United States: A Policy Statement From the American Heart Association. *Circulation, 123*(8), 933-944.

(17) JEOL (2015). *JSM 6510 series scanning electron microscope*. JSM 6510 series catalog.

(18) Kalinowski, M. B. (2013). *The Investigation of Rubidium Cellular Uptake in Renal, Heart, and Skeletal Muscle Tissues of Wiskar Kyoto Rats (Master's thesis).* Minnesota State University, Minnesota. Mankato, Minnesota.

(19) Kanji, S., & Maclean, R. D. (2012). Cardiac Glycoside Toxicity. *Critical care clinics, 28*(4), 527-535.

(20) Krebs, H. A. and Henseleit, K. (1932). Untersuchungen über die Harnstoffbildung im Tierkörper in Hoppe-Seyler's Zeitschrift für Physiol. *Chemie*, 210, 33-66.

(21) Kupriyanov VV, Xiang B, Sun J, Jilkina O. The effect of drugs modulating K^+ transport on Rb^+ uptake and distribution in pig hearts following regional ischemia: ^{87}Rb MRI study. NMR in *Biomedicine* 15:348-355, 2002.

(22) "Linoleic Acid"," Ouabain", and "Digoxins" (n.d.). *PubChem*. Retrieved March 19, 2014, from: http://pubchem.ncbi.nlm.nih.gov

(23) Liu, T., Brown, D. A., & O'rourke, B. (2010). Role of mitochondrial dysfunction in cardiac glycoside toxicity. *Journal of Molecular and Cellular Cardiology, 49*(5), 728-736.

(24) Lorgeril, M; Renaud, Serge; Salen, P; Monjaud, I; Mamelle, N; Martin, J.L.; Guidollet, J; Touboul, P; Delaye, J (1994). *"Mediterranean alpha-linolenic acid-rich diet in secondary prevention of coronary heart disease"*. Lancet 343 (8911): 8911.

(25) Mahmmoud, Y. A., & Christensen, S. B. (2011). Oleic and linoleic acids are active principles in Nigella sativa and stabilize an E2P conformation of the Na, K-ATPase. Fatty acids differentially regulate cardiac glycoside interaction with the pump. Biochimica et Biophysica Acta (BBA) - Biomembranes, 1808(10), 2413-2420.

(26) Mohrman, D., & Heller, L. (2014). Cardiovascular Function in Pathological Situation. In *Cardiovascular Physiology* (8th ed., pp. 225-230). McGraw-Hill Education.

(27) Ogborn, M. R., Nitschmann, E., Goldberg, A., Bankovic-Calic, N., Weiler, H. A., & Aukema, H. M. (2008). Dietary Conjugated Linoleic Acid Renal Benefits and Possible Toxicity vary with Isomer, Dose and Gender in Rat Polycystic Kidney Disease. *Lipids, 43*(9), 783-791.

(28) Ottolia, M., Torres, N., Bridge, J. H., Philipson, K. D., & Goldhaber, J. I. (2013). Na/Ca exchange and contraction of the heart. *Journal of Molecular and Cellular Cardiology, 61*, 28-33.

(29) Parikh, R., & Kadowitz, P. (2013). A review of current therapies used in the treatment of congestive heart failure. *Expert Review of Cardiovascular Therapy, 11.9*, 1171-1178.

(30) Pariza, M. W., Park, Y., & Cook, M. E. (2001). The biologically active isomers of conjugated linoleic acid. *Progress in Lipid Research, 40*(4), 283-298.

(31) Purdue University (n.d). *Scanning Electron Microscope*. Radiological and Enviromental Management. Obtained from: https://www.purdue.edu/ehps/rem/rs/sem.htm

(32) Subbaiah, P. V., Gould, I. G., Lal, S., & Aizezi, B. (2011). Incorporation profiles of conjugated linoleic acid isomers in cell membranes and their positional distribution in phospholipids. *Biochimica Et Biophysica Acta (BBA) - Molecular and Cell Biology of Lipids, 1811*(1), 17-24.

(33) Tro, N. J. (2010). *Principles of chemistry: a molecular approach*. Upper Saddle River, NJ: Prentice Hall.

(34) Waard, M., & Duncker, D. (n.d.). Prior exercise improves survival, infarct healing, and left ventricular function after myocardial infarction. *Journal of Applied Physiology*, 928-936.

(35) Zarogiannis S1, Liakopoulos V, Hatzoglou C, Kourti P, Vogiatzidis K, Potamianos S, Eleftheriadis T, Gourgoulianis K, Molyvdas PA, Stefanidis I. (2007) 'Effect of sodium-potassium pump inhibition by ouabain on the permeability of isolated visceral sheep peritoneum.', *Advance in Peritoneal Dialysis*, 23(43), pp. 7.

Appendices

Before examining linoleic acid's effects, several preliminary experiments were done to either to determine optimal parameters and conditions for SEM/EDS analysis. The cardiomyocyte rubidium levels in isolated cells were analyzed to validate the experimental design. Determination of most effective KeV level and spot size was done to set optimal parameters for analysis. Confirmation of the suggested Ouabain concentration's effect was also conducted to illustrate inhibition of rubidium uptake. All data for preliminary studies is described and analyzed below in the following appendices. Also included at the end of this section is the raw data for the main trial set examining linoleic acid's effects on cardiomyocyte rubidium weight percent.

Appendix A: Changes in Cellular Rubidium Levels over Time

Cells were prepared as seen in *Figure 10*. Five 15 mL tubes were labeled with the time points, and the stock of isolated cardiomyocytes was divided upon the five tubes. Samples were left to incubate and were freeze-dried when they reached the end of their time point. Samples of the time point "0.0 hours" did not incubate, and time point "2.0 hours" samples incubated for two hours, and so on. Ten cells were analyzed by SEM/EDS for each time point with the SEM electron beam set at 15 kV and a spot size of 40 nm. Rubidium weight-percent for all cells in each time point is included in *Table 5.* Averages and standard error were calculated and graphed as illustrated in *Figure 19.*

For average cardiomyocyte rubidium weight percent, time point "0.0 Hours" resulted in mean of 0.033 +/- 0.028, and a Wilk-Shapiro normal distribution p-value of 0.000. Time point "0.5 Hours" resulted in mean of 0.117 +/- 0.058, and a Wilk-Shapiro normal distribution p-value of 0.001. Time point "1.0 Hours" resulted in mean of 0.126

+/- 0.054, and a Wilk-Shapiro normal distribution p-value of 0.006. Time point “1.0 Hours” resulted in mean of 0.126 +/- 0.054, and a Wilk-Shapiro normal distribution p-value of 0.006. Time point “1.5 Hours” resulted in mean of 0.249 +/- 0.056, and a Wilk-Shapiro normal distribution p-value of 0.605. Time point “2.0 Hours” resulted in mean of 0.473 +/- 0.144, and a Wilk-Shapiro normal distribution p-value of 0.126. Only time points “1.5 Hours” and “2.0 Hours” were considered normally distributed, and time points “0.0 Hours”, “0.5 Hours”, “1.0 Hours” were considered not normally distributed. Levene’s homogeneity test of variance resulted in a p-value > 0.000, which indicates that the variance within time point cells’ rubidium percentages are not equal amongst the different time points. The ANOVA test resulted in a p-value of 0.003 indicating significant differences amongst the time point groups, which was further confirmed by the more statistically robust Welch-ANOVA’s p-value of 0.008. Significant difference between the treatment groups were identified using the Tukey post-hoc test. It indicated that time point “2.0 Hours” was significantly higher in cardiomyocyte rubidium weight percent than time points “0.0 Hours” (p=0.002), “0.5 Hours” (p=0.021), and “1.0 Hours” (p=0.025), but not time point “1.5 Hours” (p=0.278).

Table 5: Rubidium Weight Percent Values at Different Times

Cell #	0.0Hr	0.5Hr	1.0Hr	1.5Hr	2.0HR
1	0	0.33	0.22	0	1.05
2	0	0.29	0.23	0.33	1.16
3	0	0.01	0	0.4	0
4	0	0.05	0.31	0.53	0.96
5	0	0	0	0	0.13
6	0	0.49	0	0.2	0
7	0	0	0.02	0.13	0.48
8	0.05	0	0.48	0.38	0.33
9	0	0	0	0.35	0
10	0.28	0	0	0.17	0.62
Average	**0.033**	**0.117**	**0.126**	**0.249**	**0.473**
Standard Error	**0.028**	**0.058**	**0.054**	**0.056**	**0.144**

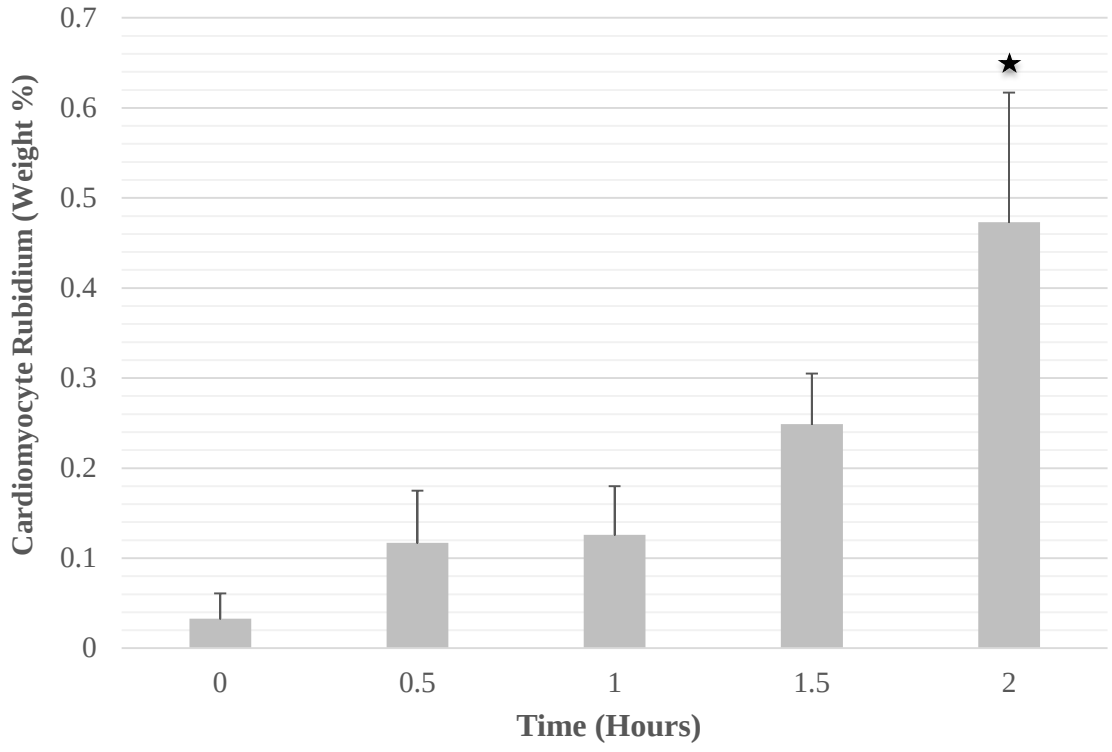

Figure 19: Cardiomyocyte rubidium levels at time intervals. Values are mean and standard error. Star indicates significant difference ($p < 0.05$) from the treatment groups 0.0 Hours.

Appendix B Optimum Electron Beam Spot Size

Cells were prepared as seen in *Figure 10.* The sample of isolated cardiomyocytes incubated for two hours in rubidium-Krebs, and then freeze-dried and prepared for SEM/EDS analysis. Six cells were picked for SEM/EDS analysis, and each cell was analyzed at spot size 20 nm, 30 nm, 40 nm, 50 nm, and 60 nm. The kV of the electron beam was set to 15 kV during the analysis of all different spot size treatment groups. Rubidium weight percent for all cells in each spot size group is included in *Table 6.* Averages and standard error were calculated and graphed as illustrated in *Figure 20.*

For average cardiomyocyte rubidium weight percent, the spot size 20 nm resulted in a mean 0.150 +/- 0.086, and a Wilk-Shapiro normal distribution p-value of 0.056. The spot size 30 nm resulted in a mean 0.095 +/- 0.034, and a Wilk-Shapiro normal distribution p-value of 0.593. The spot size 40 nm resulted in a mean 0.113 +/- 0.060, and a Wilk-Shapiro normal distribution p-value of 0.015. The spot size 50 nm resulted in a mean 0.366 +/- 0.117, and a Wilk-Shapiro normal distribution p-value of 0.858. The spot size 60 nm resulted in a mean 0.483 +/- 0.127, and a Wilk-Shapiro normal distribution p-value of 0.561. All spot size groups were considered normally distributed except the group 40 nm. Although the treatment group 60 nm for a spot size yielded the best rubidium weight percent in the analysis, it produced a distorted imaging and therefore, 50 nm was used as the standard spot size in subsequent experimental trials.

Table 6: Rubidium weight percent values with different electron beam spot sizes at 15 kV accelerating voltage

Cell #	20nm	30nm	40nm	50nm	60nm
1	0.53	0.09	0.3	0.83	0.44
2	0	0.04	0	0	0
3	0	0.05	0	0.14	0.4
4	0.12	0	0.08	0.35	0.77
5	0	0.22	0.3	0.41	0.88
6	0.25	0.17	0	0.47	0.41
Average	**0.150**	**0.095**	**0.113**	**0.366**	**0.483**
Standard Error	**0.086**	**0.034**	**0.060**	**0.117**	**0.127**

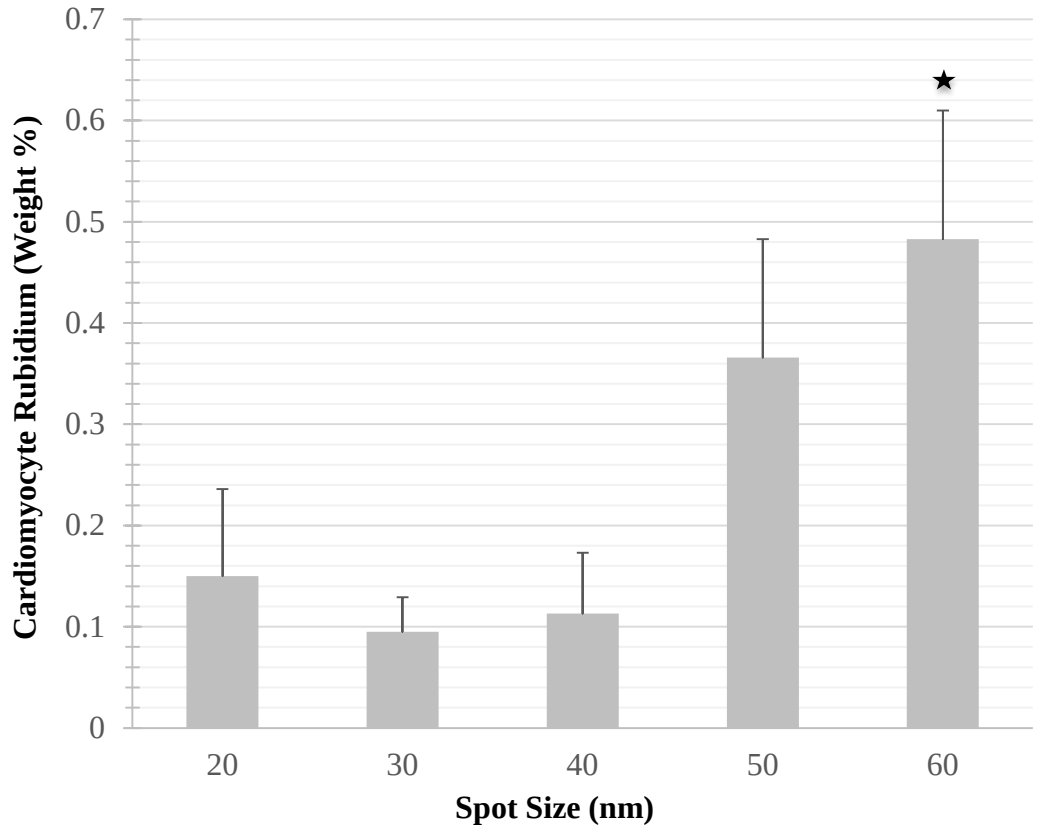

Figure 20: Cardiomyocyte rubidium levels at different SEM spot size. Values are mean and standard error. Star indicates significant difference ($p < 0.05$) from other treatment groups.

Appendix C Optimum Voltage of Electron Beam

Cells were prepared as seen in *Figure 10.* The sample of isolated cardiomyocytes incubated for two hours in rubidium-Krebs, and then freeze-dried and prepared for SEM/EDS analysis. Six cells were picked for SEM/EDS analysis, and each cell was analyzed at KeV level of 15kV. 20kV, 25kV, and 30kV. The SEM spot size was set to 40 nm during the analysis. Rubidium weight percent for all cells in each KeV level group is included in *Table 7.* Averages and standard error were calculated and graphed as illustrated in *Figure 21*.

For average cardiomyocyte rubidium weight percent, the KeV level 15kV resulted in a mean 0.433 +/- 0.135, and a Wilk-Shapiro normal distribution p-value of 0.911. The KeV level 20kV resulted in a mean 1.026 +/- 0.0.260, and a Wilk-Shapiro normal distribution p-value of 0.017. The KeV level 25kV resulted in a mean 0.016 +/- 0.017, and a Wilk-Shapiro normal distribution p-value < 0.000. The KeV level 30kV resulted in a mean 0.021 +/- 0.007, and a Wilk-Shapiro normal distribution p-value of 0.007. All KeV groups were considered to have normal distribution except 25kV. Levene's test for homogeneity of variance resulted in a p-value of 0.000, which indicated that the variance within KeV groups were not equal amongst all KeV groups. The ANOVA test resulted in a p-value of 0.000 indicating significant differences amongst the KeV groups. Using the Tukey post-hoc test, the 20kV group was found to detect significantly higher rubidium weight percent than 15kV (p=0.044), 25kV (p=0.001), and 30kV (p=0.001).

Table 7: Rubidium Weight Percent Values with Different Electron Beam Accelerating Voltages.

Cell #	15kV	20kV	25kV	30kV
1	0	0.41	0	0.02
2	0.26	0.72	0.1	0.04
3	0.25	0.44	0	0.03
4	0.92	1.34	0	0
5	0.5	1.18	0	0
6	0.67	2.07	0	0.04
Average	**0.433**	**1.026**	**0.016**	**0.021**
Standard Error	**0.135**	**0.260**	**0.017**	**0.007**

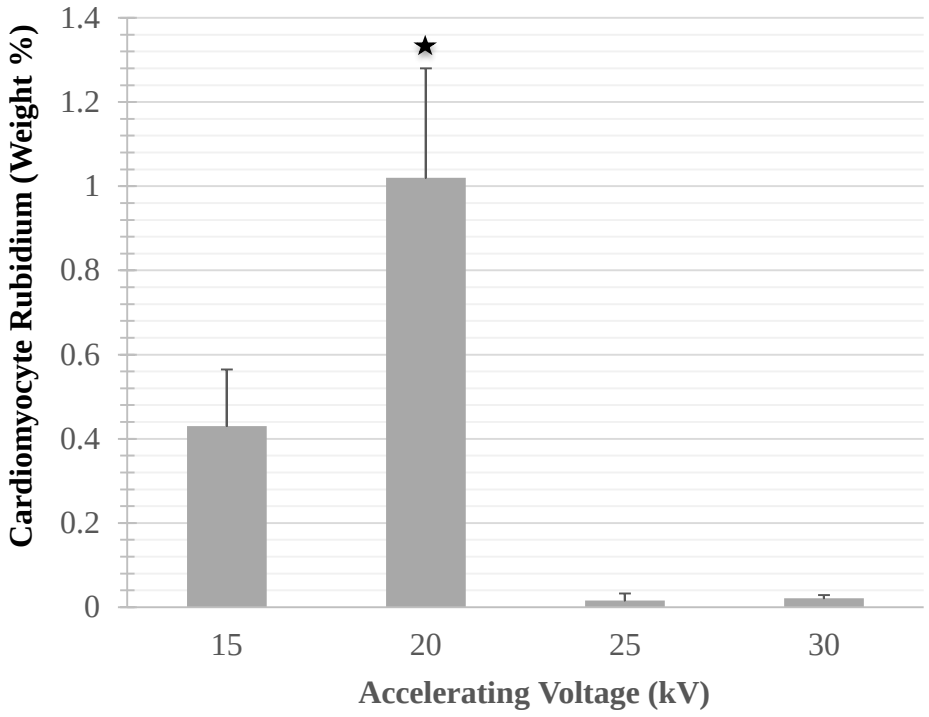

Figure 21: Cardiomyocyte rubidium levels at different SEM accelerating voltages. Values are mean and standard error. Star indicates significant difference ($p < 0.05$) from other treatment groups.

Appendix D Ouabain Inhibition of Cardiomyocyte Rubidium Incorporation

Ouabain served as a positive control for inhibition of the sodium potassium pump's incorporation of rubidium. It was suggested from the literature that 10^{-3} M of Ouabain in Krebs-buffer is ideal to induce such inhibition (35). To confirm Ouabain's effect on cardiomyocyte rubidium weight percent, cells were prepared as seen in *Figure 10.* The sample of isolated cardiomyocytes was then split in equal volume and each fraction was incubated for two hours in either "rubidium-Krebs" or in "10^{-3} M Ouabain + rubidium-Krebs". Samples were then freeze-dried and prepared for SEM/EDS analysis. 10 cells were SEM/EDS analyzed from each treatment. Rubidium weight percent for all cells in each treatment is included in *Table 8.* Averages and standard error were calculated and graphed as illustrated in *Figure 22*.

For average cardiomyocyte rubidium weight percent, cells incubated in "rubidium-Krebs" yielded a mean of 1.981 +/- 0.164, and a Wilk-Shapiro normal distribution p-value of 0.987. Cells incubated in "10^{-3} M Ouabain + rubidium-Krebs" yielded a mean of 0.294 +/- 0.120, and a Wilk-Shapiro normal distribution p-value of 0.010. The "10^{-3} M Ouabain + rubidium-Krebs" was considered to have a non-normal distribution of values. To compare the means of the two treatment groups, an independent sample t-test was performed. Levene's test for equality of variance resulted in a p-value of 0.432, which indicates that variances within cells treated in "rubidium-Krebs" and cells treated in "10^{-3} M Ouabain + rubidium-Krebs" are equal between the two treatment groups. Under the assumption of equal variances, the independent sample t-test resulted in a two-tailed p-value of 0.000. This confirms that the intracellular rubidium percentages within cells treated in "rubidium-Krebs" are significantly higher the than intracellular rubidium percentages within cell treated in "10^{-3} M Ouabain + rubidium-Krebs".

Table 8: Rubidium Weight percent values of cells treated incubated with Ouabain

Cell #	Rb Krebs	10^{-3} M Ouabain + Rb Krebs
1	1.92	0
2	1.63	0.83
3	1.75	0.62
4	2.18	0.97
5	2.57	0.13
6	2.4	0.36
7	1.93	0.03
8	1.53	0
9	1.09	0
10	2.81	0
Average	**1.981**	**0.294**
Standard Error	**0.164**	**0.120**

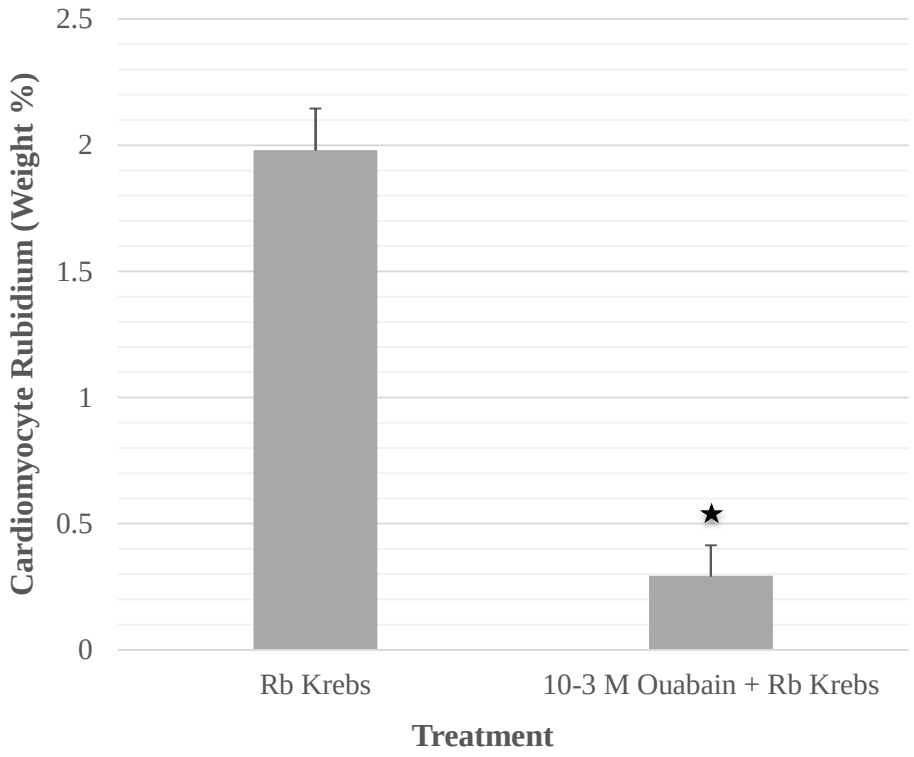

Figure 22: Effect of Ouabain (10^{-3}M) on cardiomyocyte rubidium weight percent. Values are mean and standard error. Star indicates significant difference ($p < 0.05$) from other treatment group.

Appendix E

Finally, to conclude the preliminary studies, the nature of rubidium signals detected by EDS needed to be examined. Incubated samples were prepared on coverslips obtained from *Fisher Scientific*, and those coverslips are composed of Borosilicate (8). Borosilicate makes a type of glass composed of a mixture of the elements boron and silicon. This means that EDS will detect signals from the coverslip for the elements boron and silicon. This is a significant dilemma considering that silicon is observed 1.73 kV and rubidium is observed at 1.69 kV (14). The significance of this dilemma is further exasperated considering that rubidium and silicon were observed to map in an almost identical fashion in EDS readings as seen in *Figure 5.* To overcome this challenge, a qualitative trial examining the effect of preparation surface was conducted. Isolated cardiomyocyte samples were prepared as seen in *Figure 9.* The sample of isolated cardiomyocytes was divided into two fractions. One fraction was prepared on typical *Fisherbrand*™ glass coverslips, and the second fraction was prepared on a specialized carbon stub. All other SEM/EDS parameters for the analysis were kept the same, and cells were observed in an internal view at 8,000x magnification for the presence rubidium within the cells as seen in *Figure 23*. *Figure 23* shows that rubidium was detected similarly in a cell prepared on *Fisherbrand*™ glass coverslips and a cell prepared on the specialized carbon stub.

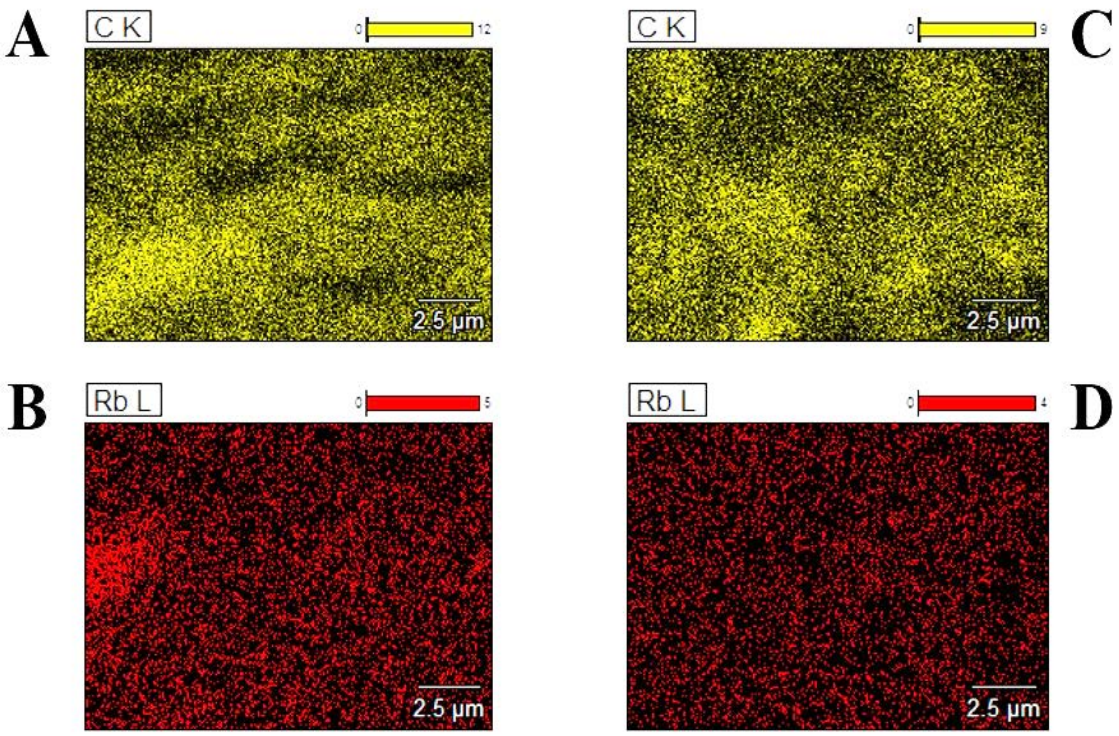

Figure 23: Map of carbon at a magnification of x8,000 showing **A)** the carbon element-print of a cell prepared on the surface of a *Fisherbrand*™ glass coverslip, **B)** the rubidium element-print of the cell in A, **C)** the carbon element-print of a cell prepared on a carbon-stub, and **D)** the rubidium element-print of the cell in C.

Appendix F Cardiomyocyte Rubidium Levels in Experimental Trials

Linoleic Acid Trial 1			
Treatment	**Cell**	**Rb (Weight**	**Treatment Average**
Rubidium	1	1.07	
Rubidium	2	0.14	
Rubidium	3	0.41	
Rubidium	4	1.82	
Rubidium	5	1.75	
Rubidium	6	1.66	
Rubidium	7	1.9	
Rubidium	8	0.55	
Rubidium	9	0.65	
Rubidium	10	0.94	**1.089** ± 0.206
Ouabain	1	0.73	
Ouabain	2	0.52	
Ouabain	3	0.71	
Ouabain	4	1.31	
Ouabain	5	1.62	
Ouabain	6	0.41	
Ouabain	7	1.08	
Ouabain	8	1.02	
Ouabain	9	1.47	
Ouabain	10	1.37	**1.024** ± 0.132
Linoleic Acid 10-3 M	1	0	
Linoleic Acid 10-3 M	2	0	
Linoleic Acid 10-3 M	3	0.07	
Linoleic Acid 10-3 M	4	2.34	
Linoleic Acid 10-3 M	5	1.91	
Linoleic Acid 10-3 M	6	1.74	
Linoleic Acid 10-3 M	7	1.62	
Linoleic Acid 10-3 M	8	2.49	
Linoleic Acid 10-3 M	9	1.65	
Linoleic Acid 10-3 M	10	2.63	**1.445** ± 0.329
Linoleic Acid 10-6 M	1	1.04	
Linoleic Acid 10-6 M	2	2.67	
Linoleic Acid 10-6 M	3	2.41	
Linoleic Acid 10-6 M	4	2.56	
Linoleic Acid 10-6 M	5	1.22	
Linoleic Acid 10-6 M	6	0.31	
Linoleic Acid 10-6 M	7	0.41	
Linoleic Acid 10-6 M	8	0.65	
Linoleic Acid 10-6 M	9	0.17	
Linoleic Acid 10-6 M	10	1.2	**1.264** ± 0.303

Linoleic Acid Trial 2

Treatment	Cell #	Rb Weight %	Treatment Rb % Average
Rubidium	1	1.62	
Rubidium	2	2.95	
Rubidium	3	1.29	
Rubidium	4	1.79	
Rubidium	5	1.65	
Rubidium	6	2.54	
Rubidium	7	2.31	
Rubidium	8	1.67	
Rubidium	9	2.75	
Rubidium	10	2.39	**2.096** ± 0.177
Ouabain	1	1.1	
Ouabain	2	0.95	
Ouabain	3	0.98	
Ouabain	4	0.27	
Ouabain	5	0.39	
Ouabain	6	0.65	
Ouabain	7	0.39	
Ouabain	8	1.83	
Ouabain	9	0.73	
Ouabain	10	0	**0.729** ± 0.165
Linoleic Acid 10-3 M	1	0.35	
Linoleic Acid 10-3 M	2	1.85	
Linoleic Acid 10-3 M	3	0.46	
Linoleic Acid 10-3 M	4	0.94	
Linoleic Acid 10-3 M	5	0.62	
Linoleic Acid 10-3 M	6	1.03	
Linoleic Acid 10-3 M	7	0	
Linoleic Acid 10-3 M	8	0	
Linoleic Acid 10-3 M	9	0	
Linoleic Acid 10-3 M	10	0.03	**0.528** ± 0.191
Linoleic Acid 10-6 M	1	0.24	
Linoleic Acid 10-6 M	2	1.51	
Linoleic Acid 10-6 M	3	0.54	
Linoleic Acid 10-6 M	4	0.16	
Linoleic Acid 10-6 M	5	0.47	
Linoleic Acid 10-6 M	6	0	
Linoleic Acid 10-6 M	7	0.64	
Linoleic Acid 10-6 M	8	0.7	
Linoleic Acid 10-6 M	9	0.35	
Linoleic Acid 10-6 M	10	0	**0.461** ± 0.140

Linoleic Acid Trial 3			
Treatment	**Cell #**	**Rb Weight %**	**Treatment Rb % Average**
Rubidium	1	2.36	
Rubidium	2	0.88	
Rubidium	3	1.49	
Rubidium	4	0.84	
Rubidium	5	1.65	
Rubidium	6	1.69	
Rubidium	7	1.32	
Rubidium	8	1.28	
Rubidium	9	1.17	
Rubidium	10	2.06	**1.474** ± 0.153
Ouabain	1	0.38	
Ouabain	2	0.35	
Ouabain	3	0.45	
Ouabain	4	0.44	
Ouabain	5	1.05	
Ouabain	6	1.1	
Ouabain	7	0.85	
Ouabain	8	0.78	
Ouabain	9	0	
Ouabain	10	0.89	**0.629** ± 0.113
Linoleic Acid 10-3 M	1	0.81	
Linoleic Acid 10-3 M	2	0.23	
Linoleic Acid 10-3 M	3	2.49	
Linoleic Acid 10-3 M	4	0.65	
Linoleic Acid 10-3 M	5	0.66	
Linoleic Acid 10-3 M	6	1.79	
Linoleic Acid 10-3 M	7	0.92	
Linoleic Acid 10-3 M	8	1.62	
Linoleic Acid 10-3 M	9	0.76	
Linoleic Acid 10-3 M	10	1.73	**1.166** ± 0.222
Linoleic Acid 10-6 M	1	0.47	
Linoleic Acid 10-6 M	2	0.1	
Linoleic Acid 10-6 M	3	1.13	
Linoleic Acid 10-6 M	4	0.12	
Linoleic Acid 10-6 M	5	0.21	
Linoleic Acid 10-6 M	6	1.93	
Linoleic Acid 10-6 M	7	0	
Linoleic Acid 10-6 M	8	0	
Linoleic Acid 10-6 M	9	0.03	
Linoleic Acid 10-6 M	10	0.26	**0.425** ± 0.199

Linoleic Acid Trial 4

Treatment	Cell #	Rb Weight %	Treatment Rb % Average
Rubidium	1	2.25	
Rubidium	2	0.25	
Rubidium	3	0.87	
Rubidium	4	1.41	
Rubidium	5	1.25	
Rubidium	6	0.47	
Rubidium	7	0.17	
Rubidium	8	1.27	
Rubidium	9	0.65	
Rubidium	10	2.29	**1.088** ± 0.239
Ouabain	1	0	
Ouabain	2	0	
Ouabain	3	0	
Ouabain	4	0.89	
Ouabain	5	0.86	
Ouabain	6	1.52	
Ouabain	7	1.55	
Ouabain	8	0.54	
Ouabain	9	0.33	
Ouabain	10	0	**0.569** ± 0.195
Linoleic Acid 10-3 M	1	2.47	
Linoleic Acid 10-3 M	2	0	
Linoleic Acid 10-3 M	3	0	
Linoleic Acid 10-3 M	4	0	
Linoleic Acid 10-3 M	5	0.87	
Linoleic Acid 10-3 M	6	0.96	
Linoleic Acid 10-3 M	7	1.38	
Linoleic Acid 10-3 M	8	0.29	
Linoleic Acid 10-3 M	9	0.86	
Linoleic Acid 10-3 M	10	0	**0.683** ± 0.254
Linoleic Acid 10-6 M	1	0.22	
Linoleic Acid 10-6 M	2	0.2	
Linoleic Acid 10-6 M	3	1.53	
Linoleic Acid 10-6 M	4	0.06	
Linoleic Acid 10-6 M	5	0	
Linoleic Acid 10-6 M	6	0.24	
Linoleic Acid 10-6 M	7	0.01	
Linoleic Acid 10-6 M	8	2.1	
Linoleic Acid 10-6 M	9	0.85	
Linoleic Acid 10-6 M	10	0	**0.521** ± 0.233

Linoleic Acid Trial 5			
Treatment	**Cell #**	**Rb Weight %**	**Treatment Rb % Average**
Rubidium	1	0.54	
Rubidium	2	1.32	
Rubidium	3	1.52	
Rubidium	4	0.37	
Rubidium	5	0.2	
Rubidium	6	0	
Rubidium	7	0.18	
Rubidium	8	0.21	
Rubidium	9	2.48	
Rubidium	10	1.81	**0.863** ± 0.270
Ouabain	1	0	
Ouabain	2	0.69	
Ouabain	3	0.52	
Ouabain	4	0.89	
Ouabain	5	0.61	
Ouabain	6	0.49	
Ouabain	7	0.22	
Ouabain	8	0.44	
Ouabain	9	0.45	
Ouabain	10	2.48	**0.679** ± 0.214
Linoleic Acid 10-3 M	1	0	
Linoleic Acid 10-3 M	2	1.29	
Linoleic Acid 10-3 M	3	_____	
Linoleic Acid 10-3 M	4	_____	
Linoleic Acid 10-3 M	5	_____	
Linoleic Acid 10-3 M	6	_____	
Linoleic Acid 10-3 M	7	_____	
Linoleic Acid 10-3 M	8	_____	
Linoleic Acid 10-3 M	9	_____	
Linoleic Acid 10-3 M	10		**----**
Linoleic Acid 10-6 M	1	1.5	
Linoleic Acid 10-6 M	2	1.92	
Linoleic Acid 10-6 M	3	1.11	
Linoleic Acid 10-6 M	4	0.37	
Linoleic Acid 10-6 M	5	1.48	
Linoleic Acid 10-6 M	6	0.66	
Linoleic Acid 10-6 M	7	2.11	
Linoleic Acid 10-6 M	8	2.45	
Linoleic Acid 10-6 M	9	1.62	
Linoleic Acid 10-6 M	10	2.14	**1.536** ± 0.211

Linoleic Acid Trial 6			
Treatment	**Cell #**	**Rb Weight %**	**Treatment Rb % Average**
Rubidium	1	1.28	
Rubidium	2	1.57	
Rubidium	3	0.67	
Rubidium	4	1.02	
Rubidium	5	0.78	
Rubidium	6	1.03	
Rubidium	7	0.82	
Rubidium	8	1.12	
Rubidium	9	0.92	
Rubidium	10	2.31	**1.152** ± 0.153
Ouabain	1	0	
Ouabain	2	0	
Ouabain	3	0.17	
Ouabain	4	0.86	
Ouabain	5	0	
Ouabain	6	1.16	
Ouabain	7	0	
Ouabain	8	0.71	
Ouabain	9	0	
Ouabain	10	0	**0.29** ± 0.140
Linoleic Acid 10-3 M	1	0	
Linoleic Acid 10-3 M	2	2.39	
Linoleic Acid 10-3 M	3	0.9	
Linoleic Acid 10-3 M	4	0	
Linoleic Acid 10-3 M	5	0.72	
Linoleic Acid 10-3 M	6	1.03	
Linoleic Acid 10-3 M	7	1.14	
Linoleic Acid 10-3 M	8	0.05	
Linoleic Acid 10-3 M	9	0.51	
Linoleic Acid 10-3 M	10	0.36	**0.710** ± 0.230
Linoleic Acid 10-6 M	1	1.19	
Linoleic Acid 10-6 M	2	0	
Linoleic Acid 10-6 M	3	0.27	
Linoleic Acid 10-6 M	4	0	
Linoleic Acid 10-6 M	5	2.16	
Linoleic Acid 10-6 M	6	2.2	
Linoleic Acid 10-6 M	7	2.26	
Linoleic Acid 10-6 M	8	0	
Linoleic Acid 10-6 M	9	2.45	
Linoleic Acid 10-6 M	10	0.44	**1.097** ± 0.338

Linoleic Acid Trial 7			
Treatment	**Cell**	**Rb Weight %**	**Treatment Rb % Average**
Rubidium	1	0.85	
Rubidium	2	1.35	
Rubidium	3	1.65	
Rubidium	4	1.53	
Rubidium	5	1.91	
Rubidium	6	1.54	
Rubidium	7	1.69	
Rubidium	8	1.34	
Rubidium	9	0.47	
Rubidium	10	0.79	**1.312** ± 0.145
Ouabain	1	0.3	
Ouabain	2	0.42	
Ouabain	3	0.24	
Ouabain	4	0.26	
Ouabain	5	0	
Ouabain	6	0.25	
Ouabain	7	0.22	
Ouabain	8	2.34	
Ouabain	9	1.48	
Ouabain	10	0.35	**0.586** ± 0.232
Linoleic Acid 10-3 M	1	0	
Linoleic Acid 10-3 M	2	0	
Linoleic Acid 10-3 M	3	2.28	
Linoleic Acid 10-3 M	4	2.2	
Linoleic Acid 10-3 M	5	0	
Linoleic Acid 10-3 M	6	2.15	
Linoleic Acid 10-3 M	7	0	
Linoleic Acid 10-3 M	8	0	
Linoleic Acid 10-3 M	9	1.89	
Linoleic Acid 10-3 M	10	0.68	**0.92** ± 0.337
Linoleic Acid 10-6 M	1	0.82	
Linoleic Acid 10-6 M	2	0.98	
Linoleic Acid 10-6 M	3	1.53	
Linoleic Acid 10-6 M	4	1.2	
Linoleic Acid 10-6 M	5	0.5	
Linoleic Acid 10-6 M	6	0.5	
Linoleic Acid 10-6 M	7	1.42	
Linoleic Acid 10-6 M	8	0.8	
Linoleic Acid 10-6 M	9	0.3	
Linoleic Acid 10-6 M	10	0.81	**0.886** ± 0.128

Linoleic Acid Trial 8			
Treatment	**Cell**	**Rb Weight %**	**Treatment Rb % Average**
Rubidium	1	0.79	
Rubidium	2	1.44	
Rubidium	3	0.81	
Rubidium	4	1.23	
Rubidium	5	2.15	
Rubidium	6	0.22	
Rubidium	7	1.65	
Rubidium	8	0.97	
Rubidium	9	0.78	
Rubidium	10	0.78	**1.082** ± 0.174
Ouabain	1	0	
Ouabain	2	0.08	
Ouabain	3	1.88	
Ouabain	4	1.03	
Ouabain	5	1.22	
Ouabain	6	0.15	
Ouabain	7	1.68	
Ouabain	8	0.42	
Ouabain	9	0	
Ouabain	10	0.86	**0.732** ± 0.223
Linoleic Acid 10-3 M	1	0.66	
Linoleic Acid 10-3 M	2	0.1	
Linoleic Acid 10-3 M	3	0.42	
Linoleic Acid 10-3 M	4	0.53	
Linoleic Acid 10-3 M	5	1.37	
Linoleic Acid 10-3 M	6	1.77	
Linoleic Acid 10-3 M	7	0.31	
Linoleic Acid 10-3 M	8	1.77	
Linoleic Acid 10-3 M	9	0.34	
Linoleic Acid 10-3 M	10	1.93	**0.92** ± 0.224
Linoleic Acid 10-6 M	1	0.62	
Linoleic Acid 10-6 M	2	0	
Linoleic Acid 10-6 M	3	0	
Linoleic Acid 10-6 M	4	0	
Linoleic Acid 10-6 M	5	1.82	
Linoleic Acid 10-6 M	6	0.31	
Linoleic Acid 10-6 M	7	0.12	
Linoleic Acid 10-6 M	8	0.11	
Linoleic Acid 10-6 M	9	0	
Linoleic Acid 10-6 M	10	1.46	**0.444** ± 0.210

Linoleic Acid Trial 9			
Treatment	**Cell**	**Rb Weight %**	**Treatment Rb % Average**
Rubidium	1	0.09	
Rubidium	2	1.26	
Rubidium	3	1.33	
Rubidium	4	0.99	
Rubidium	5	0.61	
Rubidium	6	2.27	
Rubidium	7	1.82	
Rubidium	8	1.05	
Rubidium	9	1.57	
Rubidium	10	1.37	**1.236** ± 0.193
Ouabain	1	1.89	
Ouabain	2	0.43	
Ouabain	3	2.01	
Ouabain	4	1.29	
Ouabain	5	1.42	
Ouabain	6	1.5	
Ouabain	7	0.55	
Ouabain	8	1.65	
Ouabain	9	0.18	
Ouabain	10	0.31	**1.123** ± 0.218
Linoleic Acid 10-3 M	1	0.27	
Linoleic Acid 10-3 M	2	0	
Linoleic Acid 10-3 M	3	1.14	
Linoleic Acid 10-3 M	4	1.39	
Linoleic Acid 10-3 M	5	0.76	
Linoleic Acid 10-3 M	6	0	
Linoleic Acid 10-3 M	7	1.19	
Linoleic Acid 10-3 M	8	0.52	
Linoleic Acid 10-3 M	9	1.35	
Linoleic Acid 10-3 M	10	0.39	**0.701** ± 0.171
Linoleic Acid 10-6 M	1	0	
Linoleic Acid 10-6 M	2	0.84	
Linoleic Acid 10-6 M	3	1.55	
Linoleic Acid 10-6 M	4	0	
Linoleic Acid 10-6 M	5	0.27	
Linoleic Acid 10-6 M	6	0.74	
Linoleic Acid 10-6 M	7	0.2	
Linoleic Acid 10-6 M	8	0.54	
Linoleic Acid 10-6 M	9	1.58	
Linoleic Acid 10-6 M	10	1.03	**0.675** ± 0.184

Linoleic Acid Trial 10			
Treatment	**Cell**	**Rb Weight %**	**Treatment Rb % Average**
Rubidium	1	1.87	
Rubidium	2	1.23	
Rubidium	3	0.72	
Rubidium	4	2.13	
Rubidium	5	1.7	
Rubidium	6	1.91	
Rubidium	7	0.67	
Rubidium	8	1.75	
Rubidium	9	1.94	
Rubidium	10	0.07	**1.399** ± 0.219
Ouabain	1	0	
Ouabain	2	0	
Ouabain	3	0.24	
Ouabain	4	1.54	
Ouabain	5	0	
Ouabain	6	1.22	
Ouabain	7	0.72	
Ouabain	8	1.84	
Ouabain	9	0.68	
Ouabain	10	0.3	**0.654** ± 0.213
Linoleic Acid 10-3 M	1	0.75	
Linoleic Acid 10-3 M	2	0.05	
Linoleic Acid 10-3 M	3	0.6	
Linoleic Acid 10-3 M	4	1.69	
Linoleic Acid 10-3 M	5	1.43	
Linoleic Acid 10-3 M	6	2.04	
Linoleic Acid 10-3 M	7	0.76	
Linoleic Acid 10-3 M	8	0.38	
Linoleic Acid 10-3 M	9	1.58	
Linoleic Acid 10-3 M	10	1.31	**1.059** ± 0.203
Linoleic Acid 10-6 M	1	1.31	
Linoleic Acid 10-6 M	2	1.04	
Linoleic Acid 10-6 M	3	1.72	
Linoleic Acid 10-6 M	4	0.28	
Linoleic Acid 10-6 M	5	0	
Linoleic Acid 10-6 M	6	0.2	
Linoleic Acid 10-6 M	7	1.48	
Linoleic Acid 10-6 M	8	0.55	
Linoleic Acid 10-6 M	9	0.29	
Linoleic Acid 10-6 M	10	0.62	**0.749** ± 0.189

Appendix G: Formulation of Krebs Buffer

Stock Solutions:

Stock A

-107 g of NaCl in 1 L ddH_2O

Stock B

-5.96g of KCl

-32.26g of $NaHCO_3$

-$MgCl_2$*$2H_2O$

-dissolve contents in 1 L of ddH_2O

Stock C

-$CaCl_2$*$2H_2O$

-dissolve contents in 1 L of ddH_2O

Procedure:

1. Mix 50 ml of each of Stock A, Stock B, and Stock C with 650 ml ddH_2O.
2. Add 1.9 g of 10mM HEPES
3. Add 2 g of BSA
4. Filter into a flask using paper filter.
5. Adjust pH to 7.35
6. Warm up to 37°C for usage, and store below 5°C.